Prepared By

THE ATMOSPHERIC SCIENCE DIVISION

of

THE UNIVERSITY OF TENNESSEE SPACE INSTITUTE

SPECIAL REPORT

CONTRACT NAS8-35973

"NATURAL ENVIRONMENT ANALYSIS"

January 1985

Dr. Walter Frost

Director

Atmospheric Science Division

Prepared For

NASA Marshall Space Flight Center

TABLE OF CONTENTS

LIST OF FIGURES

FIGURE PAGE

1.0 INTRODUCTION

Wind loading on the space shuttle while on the launch pad and during initial liftoff will be very complex. This wind field is associated with the mountainous and irregular terrain features surrounding the launch site. As shown in Figure 1.1, the terrain rises rapidly to the east of the launch site reaching altitudes on the order of 1000 feet above sea level. The launch site, itself, is roughly at 390 feet above sea level. To the west of the launch site is the ocean; wind from this direction will be affected by a sudden discontinuity in surface features. Channeling of the wind, flow separation, internal boundary layers with highly turbulent shear layers, and other flow phenomena associated with surface protrusion, depressions, and surface texture discontinuities will occur.

Qualitative analyses (and quantitatively to the extent possible) of the influence of these terrain features on wind loading of the space shuttle while on the launch pad, or during early liftoff, is presented in this report. Initially, the climatology and meteorology producing macroscale wind patterns and characteristics for the Vandenburg Air Force Base (VAFB) launch site are described. Also, limited field test data are analyzed, and then the nature and characteristic of flow disturbances due to the various terrain features, both natural and man-made, are then reviewed. Following this, the magnitude of these wind loads are estimated. Finally, effects of turbulence are discussed. The study concludes that the influence of complex terrain can create significant wind loading on the vehicle. Because of the limited information, it is not possible to quantify the magnitude of these loads. Thus, additional measurements and analyses are required. Presented, also, is a recommendation to obtain the necessary measurements and to accomplish the needed analytical analyses.

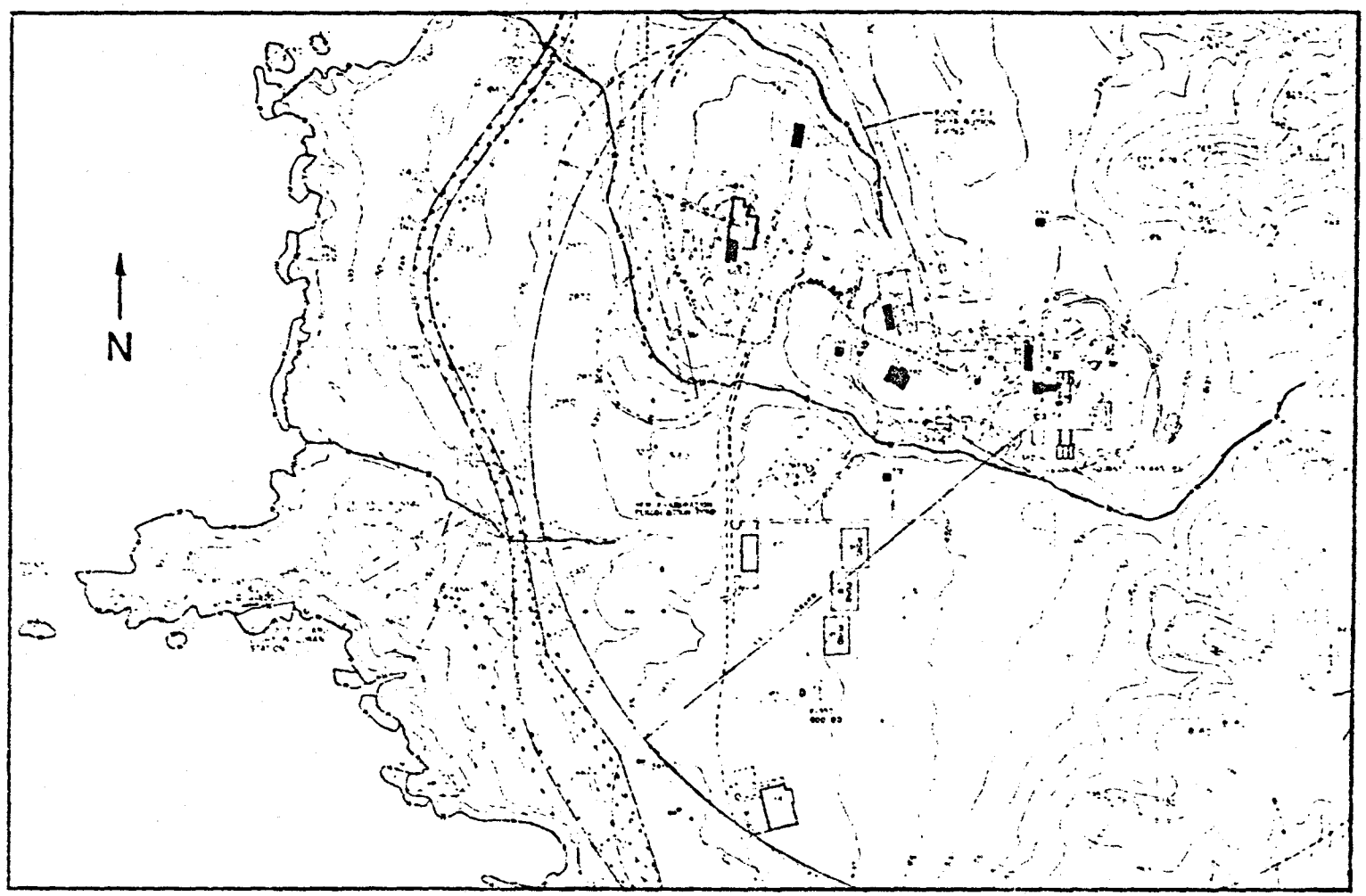

Figure 1.1. Topographical map of VAFB SLC-6 site.

2.0 GENERAL DESCRIPTION OF THE CLIMATE AND METEOROLOGY OF THE VAFB AREA

This section describes general climatology and meteorology macro-scale wind patterns and characteristics for the VAFB area. First, based on the observations of the real world, the general types of climate at VAFB are introduced. Following this, descriptions of the air circulation pattern in the upper and lower troposphere of the North Pacific, which is closely related to the formation of VAFB weather features, are made. Seasonal weather variations for Southern California are described, and the major control factors for the local weather are also interpreted. Finally, the site meteorology is reported.

2.1 General Type of Climate

The climate along the coastal area of Southern California from Monterey south to the Mexican border is categorized as a subtropical (Mediterranean) climate. This type of climate is characterized by dry dry subhimid and semi-arid zones. A strong characteristic feature of this coastal climate is the persistent night and morning stratus clouds followed by sunny afternoons. These conditions occur most often during spring and summer, with lesser frequency during the fall and winter. As a result of the moderating effect of the nearby Pacific Ocean, the coastal temperature remains comfortable all year, with very infrequent periods of temperatures above 85° F or below 45° F. Daytime winds are generally brisk and from the west, while nighttime winds are often very light, flowing toward the west and south. Severe storms, thunderstorms, and tornadoes are very rare in this area. During the fall and winter, and occasionally during late spring or early summer, strong, dry northwesterly winds (known as Santa Anas) occur.

2.2 Air Circulation Patterns

Air circulation in Southern California is influenced by the Pacific High center, cold California current, and inland topography. As shown

in Figures 2.1 and 2.2, wind directions in the upper and lower tropospheres, respectively, change with the seasons. Prevailing winter winds along the California coast are westerly in the upper troposphere and northwesterly in the lower troposphere. Summer winds are southwesterly in the upper troposphere and westerly in the lower troposphere.

A daytime sea breeze modifies the wind pattern within the lowest kilometer along the coastline. Resultant winds usually arrive from the northwest in the afternoons. Land-to-sea breezes at night are normally inhibited during the summer because of the persistent northwesterly wind at VAFB; the annual average wind speed for the coastline ranges from 6 to 13 knots (3 to 16 m/s); average minimum and maximum wind speed ranges are approximately 4 to 10 knots (2 to 5 m/s) and 10 to 16 knots (5 to 8 m/s), respectively.

The air circulation at the southeastern quadrant of the Pacific High has a descending motion which causes the air along the coastal area of Central California to be warm. This warm air combined with relatively cold ground temperatures during winter results in persistent, low-level inversions. In summer, when the Pacific High brings more westerly (and warmer) winds, near-ground inversions also occur, but not as frequently or with the intensity of winter inversion.

2.3 Seasonal Weather

Seasonal variations in the local Southern California weather are not as sharply defined as those of continental climates. In the winter there are more dramatic changes in weather conditions than at any other time of the year. Normal temperatures in winter are cooler than those in summer, except during Santa Ana wind conditions when temperatures may become abnormally high. Although cyclonic storms occur during this season, the VAFB launch site (SLC-6) area is somewhat removed from the main storm tracks. During the short spring, the weather becomes warmer, windier, more unstable, and cloudier than in the winter. March and April have the greatest frequency of windy days of the year. Surface ocean temperatures during this season are cold and keep the surface air

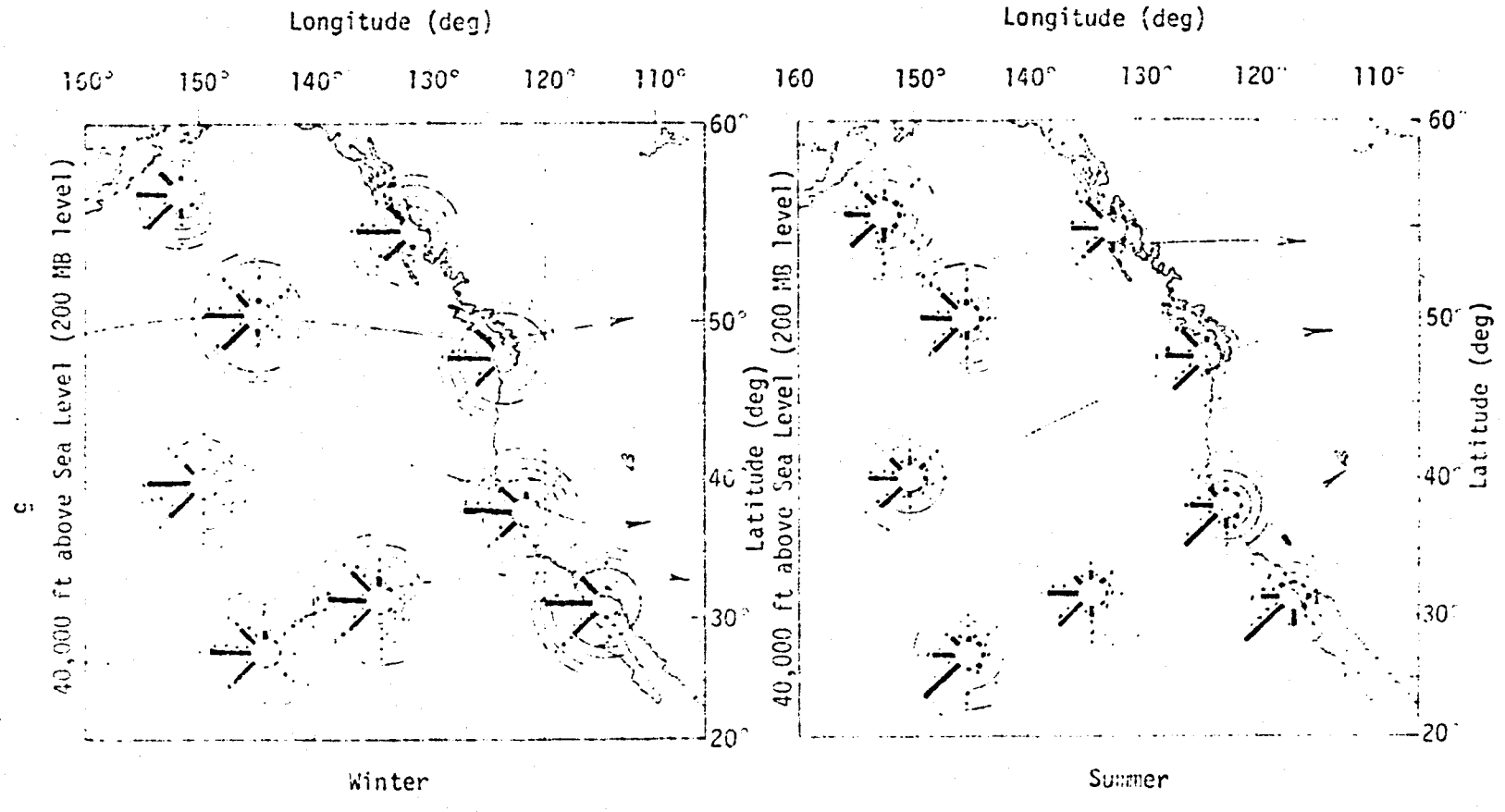

Figure 2.1. Depiction of wind directions in the upper troposphere of the North Pacific (U.S. Navy 1956).

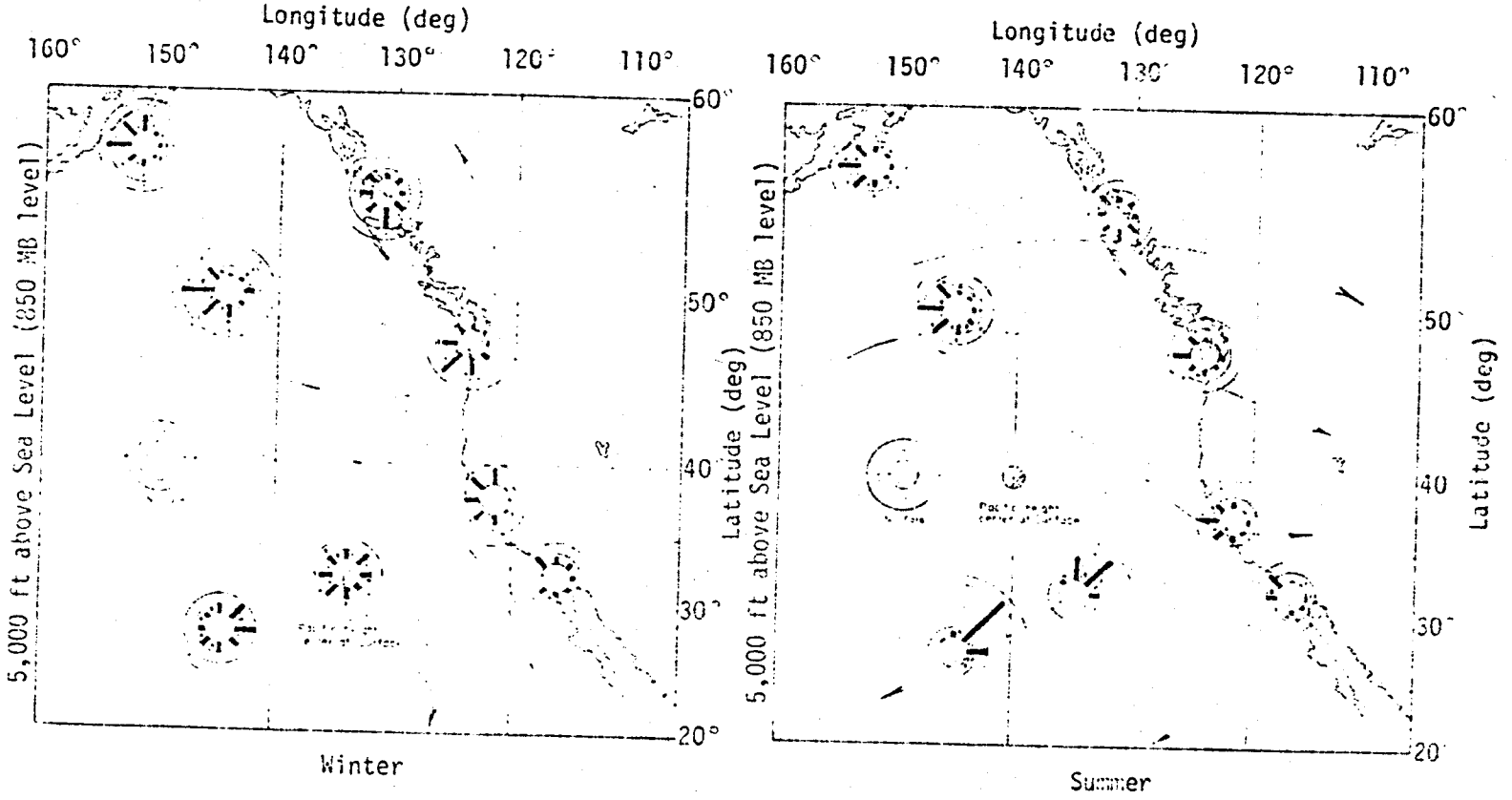

Figure 2.2. Depiction of wind directions in the upper troposphere of the North Pacific (U.S. Navy 1956).

cool. Consequently, temperature inversions, fog, and stratus clouds become more frequent, especially in late spring.

In the summer, the Pacific High center is located over the Pacific Ocean northwest of Southern California (see Figures 2.1 and 2.2). This serves to block the southward movement of low-pressure storms originating in the northern Pacific. The clockwise airflow associated with the Pacific High results in persistent northwesterly and westerly winds in offshore areas. South of Point Conception, the sea breeze component induces a more westerly wind. The low and persistent temperature inversion results in night and early morning low clouds and fog. As indicated in Section 2.1, the autumn is somewhat characterized by the Santa Ana winds.

2.4 Topographic Influence on Local Weather

Topography is a major control of site-specific climate and micro meteorology (localized weather conditions). The complicated system of mountains, valleys, points, and plains found in the project region results in a wide variation in local climatic conditions. For example, fogs are often limited to the immediate shoreline areas by the coastal mountains and proceed inland only along the valleys. The higher inland mountains, such as the Santa Ynez, Topa Topa, and Santa Monica Mountains, cause strong uplifting of marine air masses, leading to cloudiness and rain showers. The sharp coastal promontories at Point Arguello and Point Conception influence local weather conditions and are frequently shrouded in a sea fog.

2.5 Site Meteorology

This section describes in detail meteorological characteristics for the specific project sites of VAFB and Port Hueneme. Most of the general weather features such as annual averaged values of temperature, precipitation, and humidity of these sites are quite similar. However, other features such as winds are very different.

A strong temperature inversion usually accompanies the Pacific High system. This inversion caps the moist marine air about 1000 feet above the water but may be somewhat higher in summer and lower in winter. A daily height variation also occurs. Topography plays an especially important role in the height of the inversion along the VAFB coast. Under northwesterly wind conditions, the air flowing onshore and rising to the crest of the Honda ridge tends to push the base of inversion over the high ground. Thus, the inversion may be observed to slope and undulate relative to steep terrain.

Table 2.1 presents surface wind and other meteorological data for the airfield at VAFB. The annual mean surface wind speed is 6.1 knots (3.1 m/s) from a predominantly northwest direction. Monthly variations of wind show that northwesterlies persist from February through November, while southeasterlies occur during December and January. Maximum gusts of wind up to 41 knots (21 m/s) may be expected during the months of January, February, and March. Figure 2.3 illustrates seasonal variations in day- and nighttime wind directions for the Vandenberg-Point Conception region.

Wind speeds and directions are greatly influenced by the Pacific High system and the seasonal low-pressure center which forms over the Southern California deserts during the late spring and summer. The unequal daytime solar heating over land and ocean gives rise to the consistent and prevailing northwesterly low-level wind regime during most afternoons. The winds become light and variable in direction during most nights and mornings year round. Daily average wind speeds can range from nearly calm just before sunrise to upwards of 12 knots (6 m/s) by sunset. Approaching fronts and storms during the winter are the major causes disrupting this surface wind regime.

Wind speeds and directions over VAFB vary greatly as a result of the widely varying terrain. In general, wind speeds are stronger on the higher ground, along the beaches, and on Sudden Ranch. It is of particular interest that the maximum average diurnal wind speed (about 15 knots (8 m/s) at 3:00 p.m.) at southern VAFB is greater than that at the northern part of VAFB (about 6 knots (3 m/s) at 4:00 p.m.).

TABLE 2.1. Vandenberg Air Force Base, Airfield Meteorological Data (Meteorology Research, Inc. 1975).

Month	Temperature (°F)					Precipitation (inches)			Surface wind (knots)			Other	
	Mean maximum	Mean minimum	Mean monthly	Extreme maximum	Extreme minimum	Monthly maximum	Monthly minimum	Monthly mean	Prevailing direction	Mean velocity	Maximum gust	Relative humidity monthly mean (%)	% of observations with fog
Jan	61	43	51	83	28	9.30	0.89	2.16	ESE	6.2	41	68	8.1
Feb	60	44	52	84	31	9.21	0.08	2.60	NW	6.4	41	73	12.2
Mar	59	45	52	79	31	7.02	0.02	2.25	NW	7.7	40	75	12.1
Apr	61	47	53	90	36	4.03	0.01	1.25	NW	7.3	36	78	14.2
May	60	48	54	93	37	0.36	Trace[b]	0.11	NW	7.9	35	81	21.2
Jun	63	50	56	97	41	0.19	Trace[b]	0.03	NW	6.2	32	83	30.4
Jul	64	52	57	85	45	0.05	Trace[b]	0.01	NW	4.9	28	85	46.1
Aug	66	53	59	96	45	0.27	Trace[b]	0.05	NW	4.7	28	85	44.9
Sep	67	53	59	100	41	0.60	None	0.20	NW	5.0	32	82	32.0
Oct	68	51	60	99	35	3.55	Trace[b]	0.61	NW	5.3	35	75	26.2
Nov	64	47	56	87	32	6.26	None	2.06	NW	5.9	38	72	13.7
Dec	62	44	53	87	26	5.62	0.16	1.37	ESE	5.8	38	69	11.4
Mean	63	48	55	100	26	-	-	Total 12.70	NW	6.1	-	77	22.1

[a]Period: 1958-1970

[b]Trace = Less than 0.005 in.

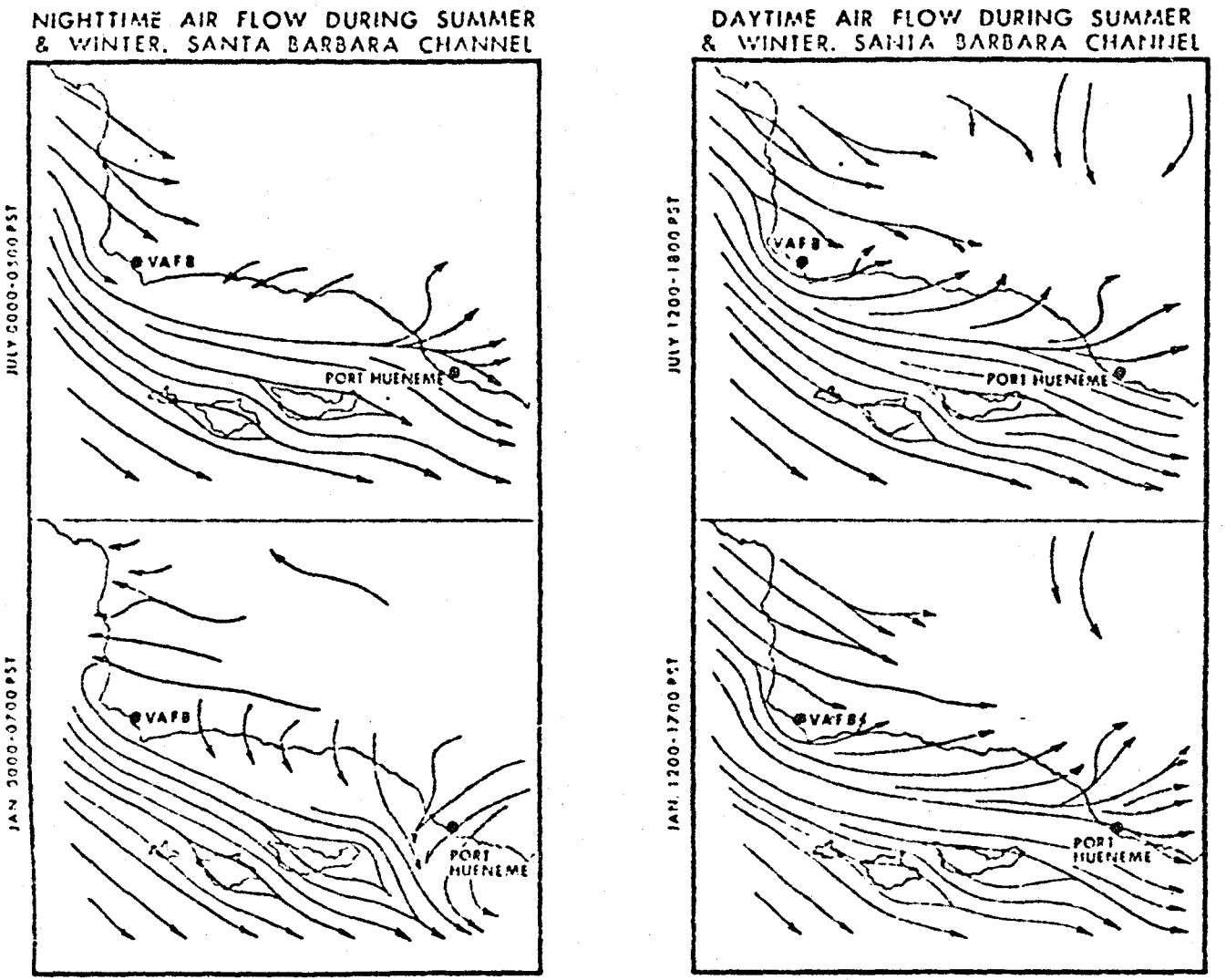

Figure 2.3. Diurnal and seasonal airflow in the VAFB vicinity (DeMarrais et al. 1965).

Table 2.2 presents average speeds and most frequent wind directions for winds aloft in the Vandenberg region. The table summarizes the vertical wind structure in 1000-foot intervals from the surface to 5000 feet. As observed at the VAFB airfield, northwesterly and occasional easterly winds are prevalent at low elevations; however, northerly and northeasterly flows frequently exist at the higher levels as shown in the table.

Surface wind and other meteorological data for Point Mugu are presented in Table 2.3. On an annual basis, surface wind direction ranging from westerly through northerly predominates, with surface wind speeds ranging from 3 to 10 knots (1.5 to 5 m/s). Seasonal variations in day- and nighttime wind directions are illustrated in Figure 2.3.

Fair-weather surface winds during the cool season are predominantly the land and sea breezes, and are not marked by winds of great intensity. The sea breeze begins in late morning and reaches a maximum intensity of approximately 10 to 15 knots (5 to 7.5 m/s) during the afternoon hours. By evening, the sea breeze is gradually replaced by a land breeze. This offshore wind, normally less than 3 knots (1.5 m/s), stops within two hours after sunrise. A broad, westerly wind is usually observed aloft.

TABLE 2.2. Average Speeds and Most Frequent Wind Directions for Winds Aloft VAFB.[a] (From U.S. Weather Bureau and California State Department of Health, 1962.)

Local standard time (PST)		Height	Average wind speed (knots) for most frequent wind direction cases												
			Jan.	Feb.	Mar.	Apr.	May	June	July	Aug.	Sept.	Oct.	Nov.	Dec.	Mean
	0400 (4 A.M.)	5,000 ft	N/20	N/21	N/22	N/19	N/19	N/14	N/12	SE/9	N/14	N/17	N/18	N/18	N/17
		4,000 ft	N/17	N/19	N/18	NE/17	N/16	N/14	NE/12	NE/10	N/12	N/16	N/15	N/18	N/15
		3,000 ft	N/15	N/16	N/16	NE/18	NE/15	N/14	NE/12	NE/10	NE/12	N/13	N/13	N/15	N-NE/11
		2,000 ft	NE/14	N/14	N/14	N/16	N/14	N/11	N/9	N/10	N/9	NE/14	N/11	NE/15	N/13
		1,000 ft	NE/11	NE/10	N/13	NW/13	NW/13	N/7	NW/7	NW/7	N/7	N/10	NE/9	NE/9	N/10
		Surface	E/6	E/5	NW/9	NW/8	NW/9	NW/6	NW/6	NW/5	NW/6	E/6	E/6	E/6	NW-E/7
	1600 (4 P.M.)	5,000 ft	N/20	N/19	N/17	N/16	N/17	NE/12	NE/9	NE/9	NE/11	N/14	N/15	N/17	N-NE/15
		4,000 ft	N/16	NW/15	N/15	NW/14	N/14	NW/11	NW/10	NW/10	NW/11	N/13	N/14	N/14	N-NW/13
		3,000 ft	N/13	NW/14	N/14	NW/14	NW/16	NW/13	NW/11	NW/11	NW/11	NW/12	N/14	N/11	N-NW/13
		2,000 ft	N/13	NW/15	NW/17	NW/17	NW/19	NW/14	NW/12	NW/11	NW/12	NW/14	NW/12	NW/12	NW/14
		1,000 ft	NW/12	NW/14	NW/18	NW/16	NW/17	NW/13	NW/10	NW/11	NW/12	NW/14	NW/13	NW/11	NW/13
		Surface	NW/11	NW/12	NW/14	NW/15	NW/14	NW/13	NW/10	NW/10	NW/11	NW/12	NW/11	NW/9	NW/12

[a]Period: 1957-1962 in Santa Maria and Point Arguello areas.

TABLE 2.3. Point Mugu Surface Climatological Data[a] (Lea 1969).

Month	Temperature (°F)					Precipitation (inches)			Surface wind (knots)			Other	
	Mean maximum	Mean minimum	Mean monthly	Extreme maximum	Extreme minimum	Monthly maximum	Monthly minimum	Monthly mean	Prevailing direction	Mean velocity	Maximum gust	Relative humidity monthly mean (%)	Mean sky coverage (%)
Jan	62	44	54	88	29	11.57	0.02	2.57	N	4	47	67	41
Feb	63	45	55	89	27	13.85	Trace[b]	2.01	N	4	38	69	43
Mar	62	45	55	87	34	4.52	Trace[b]	1.21	W	9	43	73	44
Apr	63	48	58	99	34	4.23	Trace[b]	0.97	W	10	50	77	42
May	65	51	59	96	39	0.99	Trace[b]	0.13	W	8	39	78	48
Jun	67	54	61	100	43	0.26	Trace[b]	0.03	W	8	29	81	58
Jul	70	57	63	88	41	0.13	Trace[b]	0.01	W	7	27	83	51
Aug	71	57	65	95	46	0.12	Trace[b]	0.01	W	8	24	82	51
Sep	72	57	64	97	39	0.57	Trace[b]	0.06	W	7	37	79	48
Oct	70	53	61	104	38	0.90	Trace[b]	0.19	W	7	43	77	44
Nov	68	49	59	98	31	6.42	Trace[b]	1.85	N	4	41	68	47
Dec	64	46	54	89	28	4.13	Trace[b]	0.05	N	4	42	63	40
Mean	66	51	59	104	27	-	-	Total 10.55	W	8	-	75	46

[a]Period: 1946-1971

[b]Trace = Less than 0.005 in.

3.0 ANALYSIS OF EXISTING FIELD DATA

Surface wind data is available from a number of towers located on VAFB as illustrated in Figure 3.1. The format of the data and the information available is given in Figure 3.2. Data is available on tape for 15-second averages and longer term averages (5 minutes, 15 minutes, or 1 hour). Not all of the available data has yet been put on tape. This work is being carried out by Gordon Schocker (1984) at the Naval Post-Graduate School in Monterey, California. Schocker is also analyzing the data for turbulence intensity values for use in diffusion modeling. The data has not been analyzed as to information relative to terrain effects on wind loading of the STS.

Preliminary analysis of the data has been carried out by Frost and Frost (1984). They have computed correlations of wind speeds between the different towers and at the different levels for which information is available. The results of this analysis are shown in Figure 3.3. This very preliminary data does show that certain towers are highly correlated with one another, particularly those along the coastal regions with fetch unaffected due to terrain. Inland towers, however, do not correlate well. This result can also be related to the influence of terrain features between respective towers. The influence of terrain features on the internal boundary layer is discussed in Section 7.0. These correlations will obviously depend on synoptic wind fields for which data should be available from the NOAA data repository in Asheville. This analytical study should be continued to investigate indepth what information can be obtained from individual towers. Considerably more data is available from those towers further from the SLC-6 than the 301 tower which has recently been erected at the VAFB launch site. The information will then provide greater historical data sets which can be used to understand the influence of the terrain surrounding the launch site on wind loading.

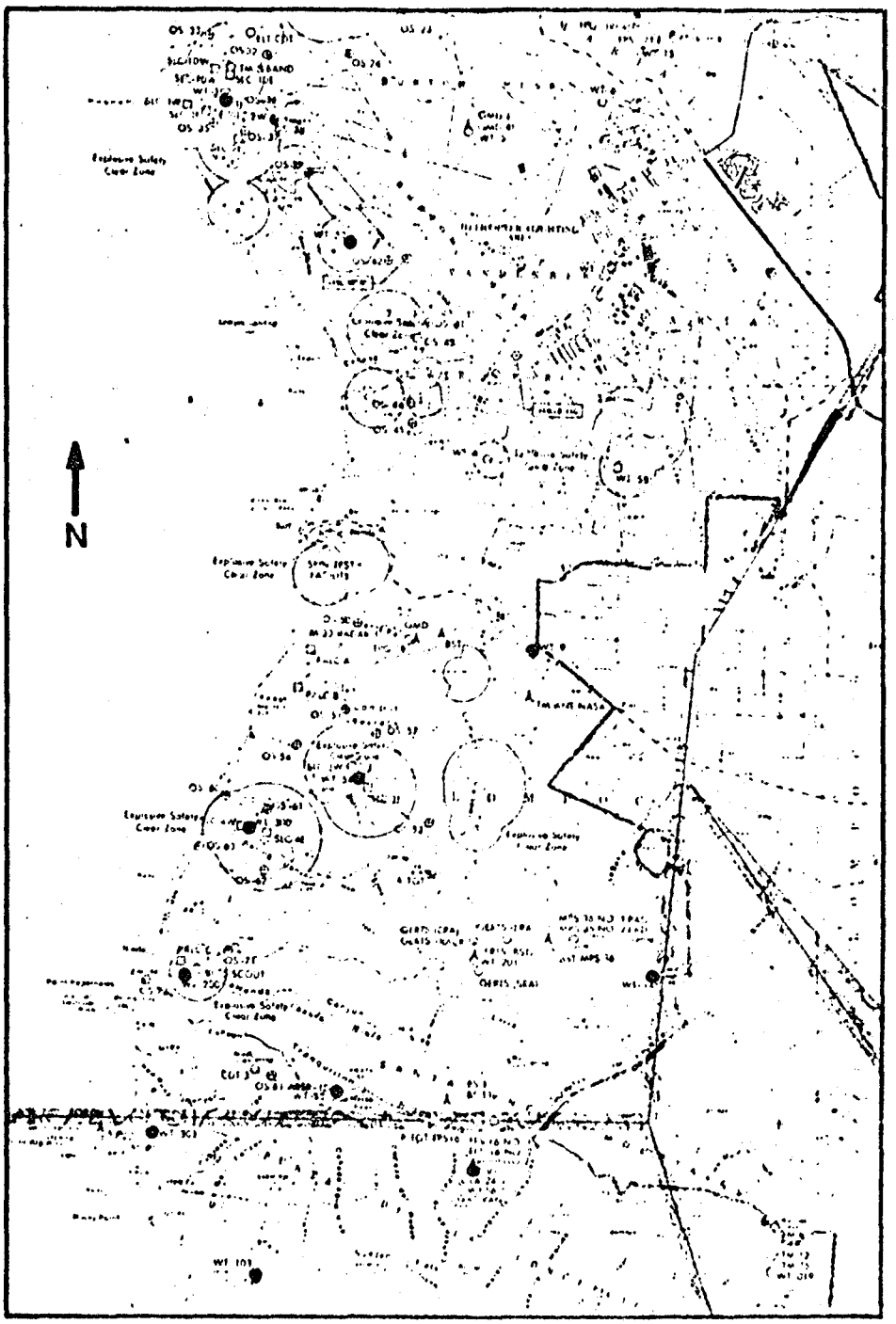

Figure 3.1 Tower location distribution on VAFB site.

General Information: Tapes, which are recorded with record size, 366 bytes (183 words), and block size, 4026 bytes (11 records) are in binary format. Four types of records, 15-second averaged data and longer term averaged data (5 minutes, 15 minutes, or 1 hour) are distinguished by the indication codes 11, 55, 15, and 66, respectively.

Each Record's Words are as Follows:

Word	15-sec Average Records	Longer Term Average Records
1-30	x-comp wind	wind speed
31-60	y-comp wind	wind direction
61-90	σ_x	σ_v
91-120	σ_y	wind counter
121-150	xy for wind	121-154 other sensors
151-180	wind counter	155-179 sensor counter
181	min., sec.	date
182	day, hour	hour, min.
183	code = 11	code = 55, 15, or 66

The Sensors that Various Data Words Correspond to are as Follows:

Word	All Records Tower/Sensor	Word	Longer Term Average Records Tower/Sensor
1	009/wind 12'	121	052/temp 6'
2	014/ "	122	054/ "
3	052/ "	123	055/ "
4	054/ "	124	056/ "
5	101/ "	125	101/ "
6	102/ "	126	102/ "
7	103/ "	127	103/ "
8	200/ "	128	200/ "
9	300/ "	129	300/ "
10	301/ "	130	301/ "
11	052/wind 54'	131	052/temp diff 54'
12	054/ "	132	054/ "
13	055/wind 40'	133	055/ "
14	056/ "	134	101/ "
15	101/wind 54'	135	102/ "
16	102/ "	136	103/ "
17	103/wind 54'	137	200/ "
18	200/ "	138	300/ "
19	300/ "	139	301/ "
20	301/ "	140	300/temp diff 102'
21	102/wind 102'	141	301/temp diff 102'
22	200/ "	142	200/temp diff 204'
23	300/ "	143	300/ "
24	299/wind 108'	144	301/ "
25	301/wind 102'	145	300/temp diff 300'
26	200/wind 204'	146	301/ "
27	300/ "	147	301/dew pt 6'
28	301/ "	148	301/dew pt 54'
29	300/wind 300'	149	301/dew pt 102'
30	301/ "	150	301/dew pt 204'
		151	301/dew pt 300'
		152	301/visibility
		153	301/barometric pressure
		154	301/short wave radiation

Conversion Factors:

R is the value from the tape after applying the factor of 10 conversion.

Wind Speed	WS	= 0.04248 R	Kts
Wind Direction	WD	= R	deg
Temperature	T	= 120 - 0.05859 R	°F
Temp. Difference	TD	= -10 + 0.02441 R	°F
Dew Point	DP	= -80 + 0.09766 R	°F
Visibility	V	= 50/(R + 1)	mi
Baro Pressure	BP	= 909.2 + 0.07988 R	mB
Radiation	SW	= 0.0009766 R	langs

Figure 3.2. Data format of the VAFB towers.

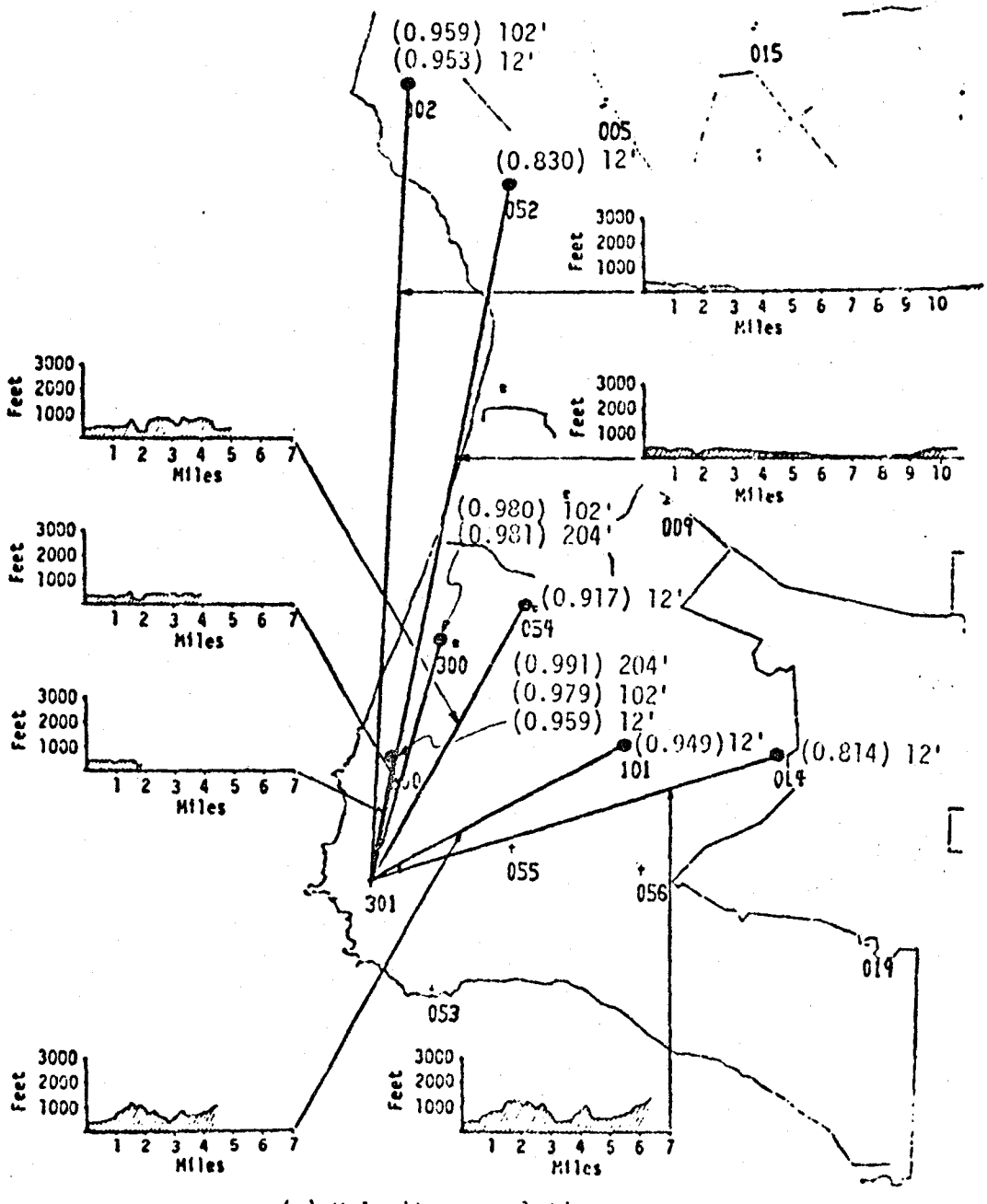

(a) Velocity correlation

Figure 3.3. Correlation.

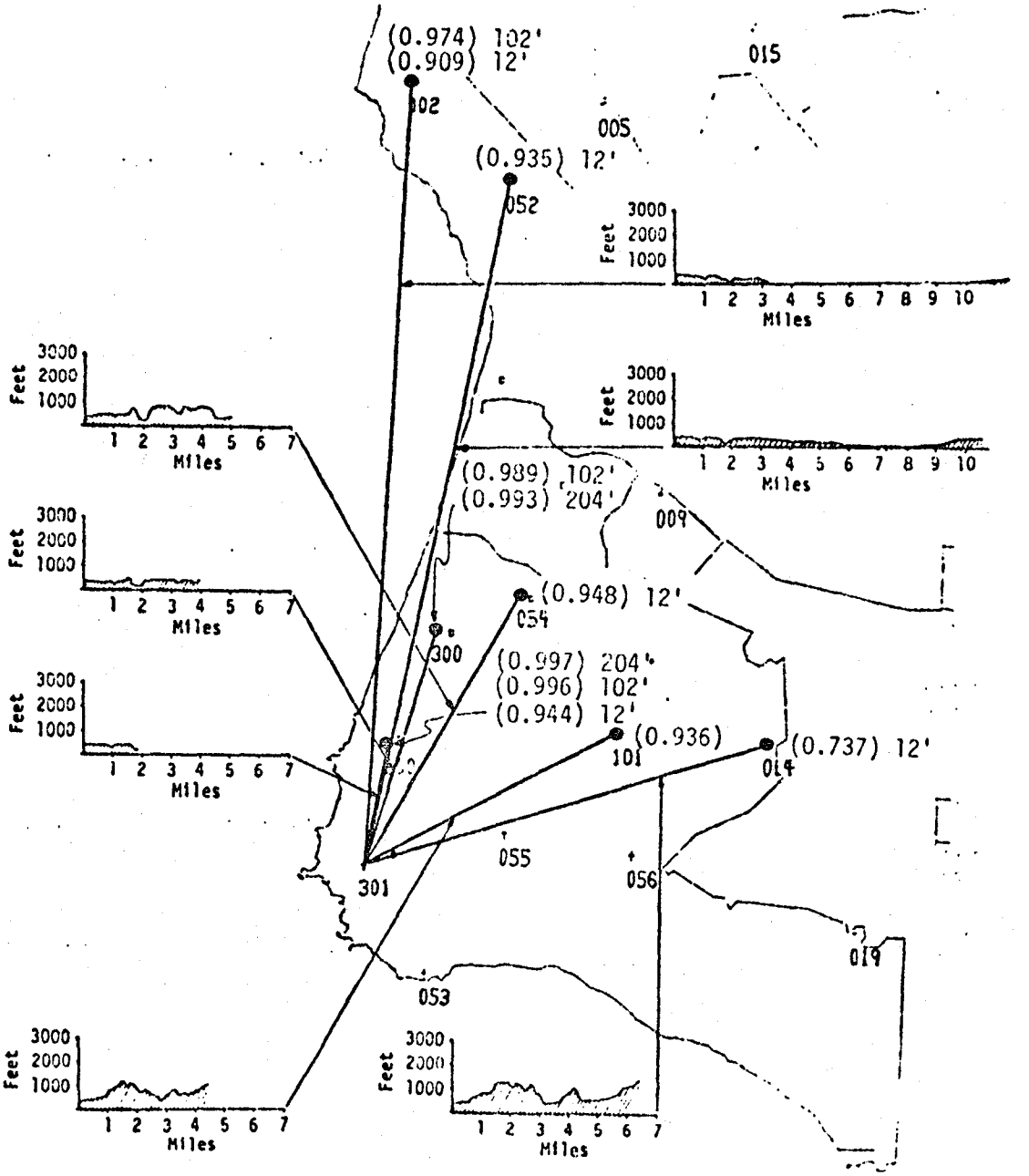

(b) Direction correlation

Figure 3.3. (continued).

4.0 CHARACTERISTIC OF FLOW DISTURBANCES

The basic types of terrain forms are protrusions, depressions, and surface discontinuities. Examples of protrusions are hills, cliffs, ridges, buildings, trees, and shelterbelts; examples of depressions are valleys, riverbeds, and canyons. Surface discontinuities are changes in surface roughness or surface thermal properties; e.g., typical examples are meadows surrounded by seashores, forests, and lakeshores. Combinations of protrusions and depressions also occur in nature, such as mountain passes, gaps in shelterbelts, and in ridges.

Frost and Shieh (1981) have reported the general characteristics of flow patterns over many terrain features. In this section, the characteristics of the flow disturbances over several interesting natural and man-made terrain features are reviewed.

The flow field around surface protrusions on flat terrain is characterized essentially by two flow features that are important to the STS while on the launch pad, or during early stages of liftoff: (a) separation of the flow, and (b) generation of vortices. Flow separation and vortices generally represent regions of pulsating or periodic flows and high turbulence. Therefore, STS launched at the site which is shrouded in these regions can have significant wind loadings.

4.1 Flow Separation

When streamlines around an object no longer follow the contour of the body, the primary flow is said to separate from the object and a reversed eddy-type flow occupies the space between the separated streamline and the object (Figure 4.1). Flow separation occurs most frequently downstream of a hill. However, it will also occur upstream if the windward slope is relatively steep. Upstream flow separation is caused by the interaction of a positive pressure gradient (pressure increasing in the flow direction) and viscous forces. Downstream separation, although also possibly caused by the same interaction that causes upstream flow separation, is more often produced by the inability of the flow to negotiate

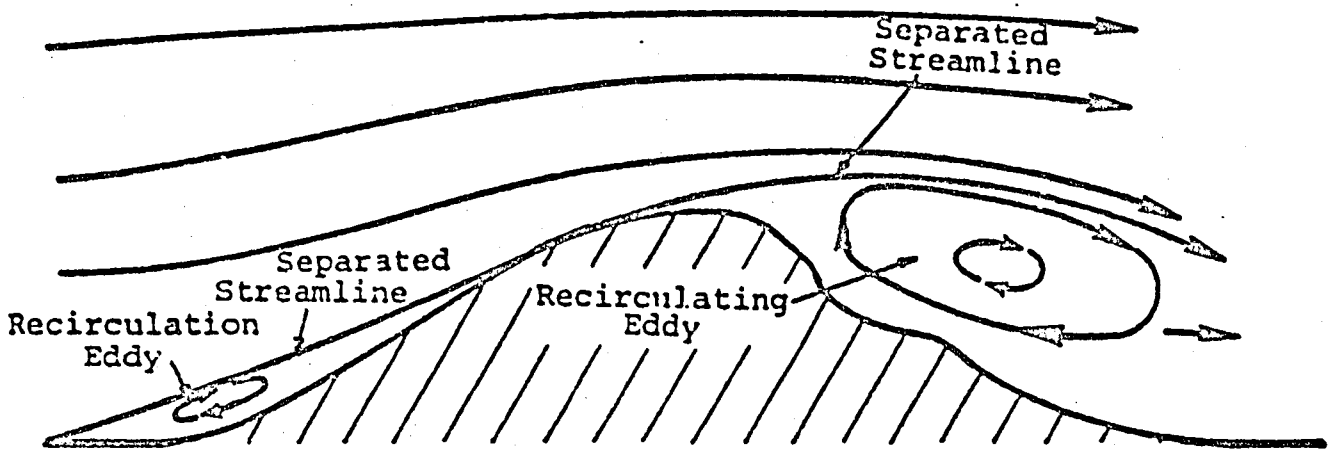

Figure 4.1. Flow separation.

a sharp change in body configuration. The physical mechanisms associated with each of these separation phenomena include positive pressure gradients, viscous interactions and sharp changes in terrain.

4.1.1 Separation Due to Positive Pressure Gradient and Viscous Interaction

Flow separation results from the interaction of an adverse pressure gradient and viscosity. The fluid particles close to the body surface have low velocity due to friction and hence insufficient momentum to overcome the adverse pressure gradient. Once these particles have lost all momentum, their flow direction will reverse and they will flow in the direction of decreasing pressure. A region of reverse flow, which increases in size as the flow propagates downstream is created. Similar results occur for a gradual but steady convex curvature, such as the downstream part of a curved hill. For a convex curvature, retardation of the main flow stream results in a static pressure rise, which causes the adverse pressure gradient. For concave curvature, the adverse pressure gradient is produced by the conversion of velocity pressure head to static pressure head, due to the deflection of the flow.

4.1.2 Separation at Sharp Changes in Terrain Configuration

Figure 4.2 illustrates flow separation caused by the flow field's inability to negotiate sudden changes in the terrain configuration. Separation thus occurs at the sharp leading edge. The mechanism of separation in this case is the high momentum of the fluid approaching the sharp leading edge. The separated flow forms a shear layer of low static pressure and high vorticity, which is bent downwind through interaction with the transverse main flow and forms an essentially parabolic shell which reattaches some distance downstream. Momentum in the separated layer diffuses into the wake and into the quasi-potential flow outside the wake, setting the wake fluid into motion and smoothing out the sharp velocity discontinuity. Following reattachment, this diffusion gradually thickens the shear layer until the inner flow is blended with the outer flow, forming a new and thicker boundary layer well downstream. The flow field for purposes of discussion and analysis may be divided by a mean separating streamline, $\psi = 0$, into an outer zone through which the

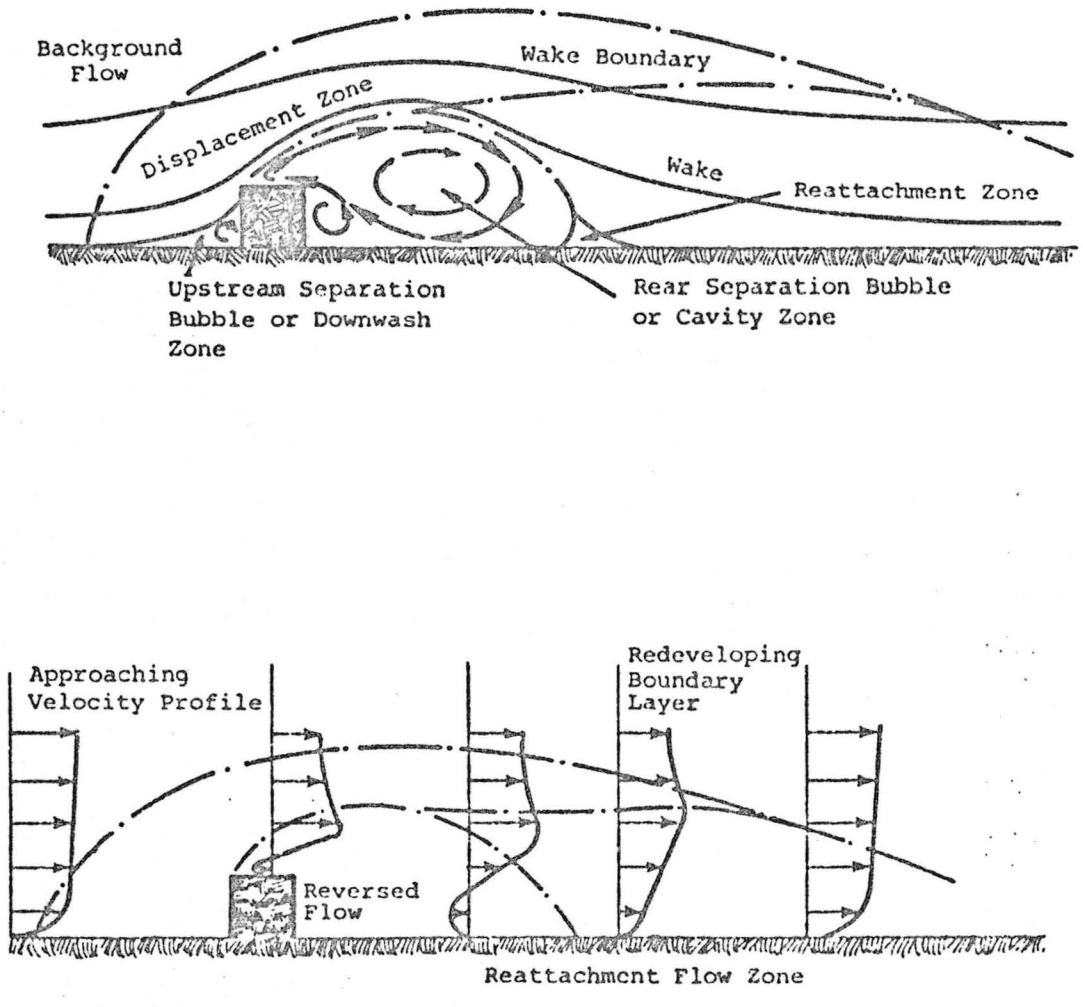

Figure 4.2. Illustration of flow separation from sharp leading edges of block terrain features.

main flow passes and an inner wake where stagnant fluid recirculates as a large eddy.

For three-dimensional flows, the separated flow pattern is even more complicated. Three-dimensional separated flow contains all the features of two-dimensional separated flow plus the effect of stretching of mean flow vorticity interpreted in the following sections.

4.1.3 Point of Separation

The longitudinal position on the terrain surface beyond where reverse flow occurs is identified as the separation point. In turbulent flow, this point of separation fluctuates and only can be identified by a mean value. For two-dimensional geometries, the separation point will occur at different locations depending on the magnitude of the upwind and downwind slopes, the stability of the atmosphere, the surface roughness, and the wind speed.

The character of flow separation occurring at the upwind side of the hill can be different from that on the downwind side as described earlier. Usually, momentum-induced separation occurs at the crest on the rearside of a triangular hill (Figure 4.3). The upstream separation region does not, in general, extend further than two hill heights, H, and occurs typically if H/L_u is greater than one half. L_u is the upwind horizontal distance from the crest of the protrusion to the location where the height of the hill is equal to 0.5 H and L_d is the downwind horizontal distance.

Meroney, et al. (1978) shows that flow separation over triangular ridges immersed in a typical shear layer profile depends strongly on H/L_d and H/L_u. Based on a series of measurements of flow over triangular hills of alternate upwind and downwind slopes, they propose the criterion for flow separation at the crest as shown in Figure 4.3. For relatively gentle downwind slopes, only weak eddies develop. This causes early reattachment of the separating streamline. For strong eddies, however, the downwind separation region interacts strongly with the main flow producing an extended wake in the downstream.

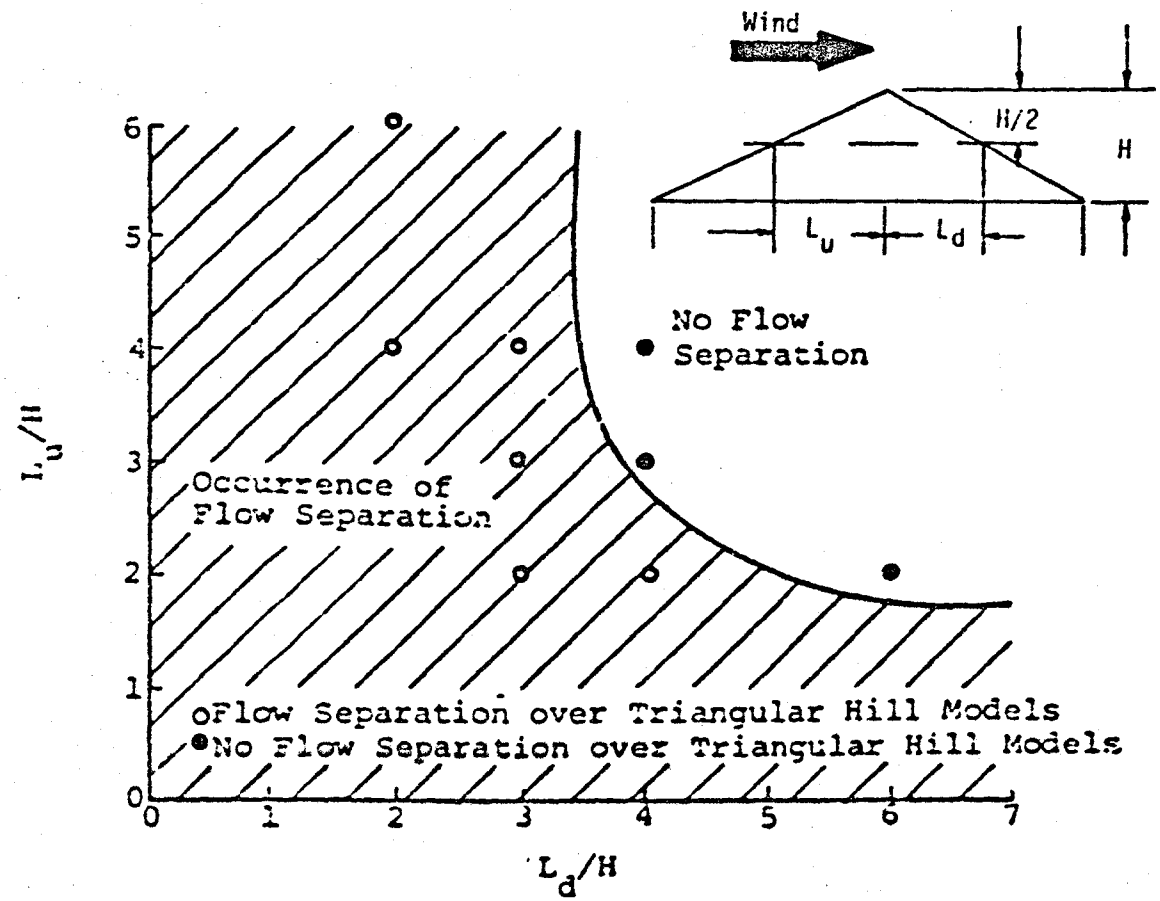

Figure 4.3. Criterion for flow separation over two-dimensional triangular hills.

4.1.4 Observation of Physical Phenonena

Figure 4.4 is a classical illustration (Yoshino 1975) of the occurrence of flow separation over natural terrain made evident by the wind-shaped tree formations on both sides of a ridge of Mt. Azuma in central Japan. Deformed trees (D) on the windward side of the prevailing wind, symmetrically formed trees (S) just behind the ridge, and deformed trees which show the opposite direction (OD) to the prevailing wind are shown on this figure. It is thought that the eddy formed behind the ridge is the cause of this situation. The eddy is not formed exactly on the x-z plane but has some twisted character under the influence of microtopography.

4.2 Vortices

Vortices associated with separated flow will have an important influence on STS launching since they are sources of high and long-lasting turbulence. Figure 4.5 shows the positions of the man-made high buildings around the VAFB (SLC-6) launch site. How complicated are the flow patterns and associated vortex shedding around a rectangular block geometry are shown in Figure 4.6, which represents flow perpendicular to the face of a block. The flow pattern becomes appreciably different when the flow is not perpendicular to a specific face of a body.

When wind blows onto a corner of a rectangular object with a single sloping top (Figure 4.7), a vortex forms along the leading surface. The tip of the vortex attaches to the upstream corner; the cone of the vortex lies roughly along the leading edge of the top. If the slope of the top is large, the vortex sheet is tightly spiraled into a strong, conical vortex whose pressure field may be severe. Further, if the vortex swings or changes in intensity (i.e., pulsates), as it may do in a natural wind, a pulsating wind field results.

The vortices shed from the hills have typically a helical structure. Their cone is fast-rotating with an axial flow velocity component and is often subject ot bursting, whereby their diameter is greatly enlarged. The outer flow regions resemble potential vortex flow,

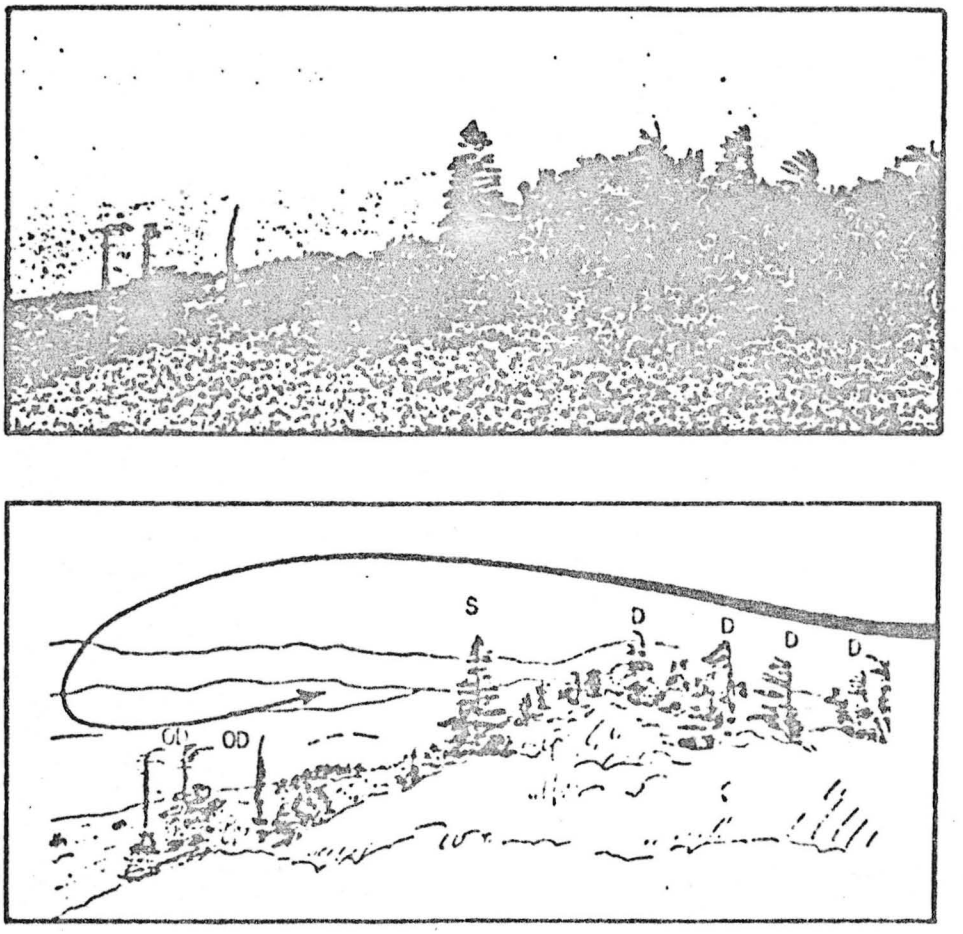

Figure 4.4. Physical visualization of separation phenomena (Yoshino 1975).

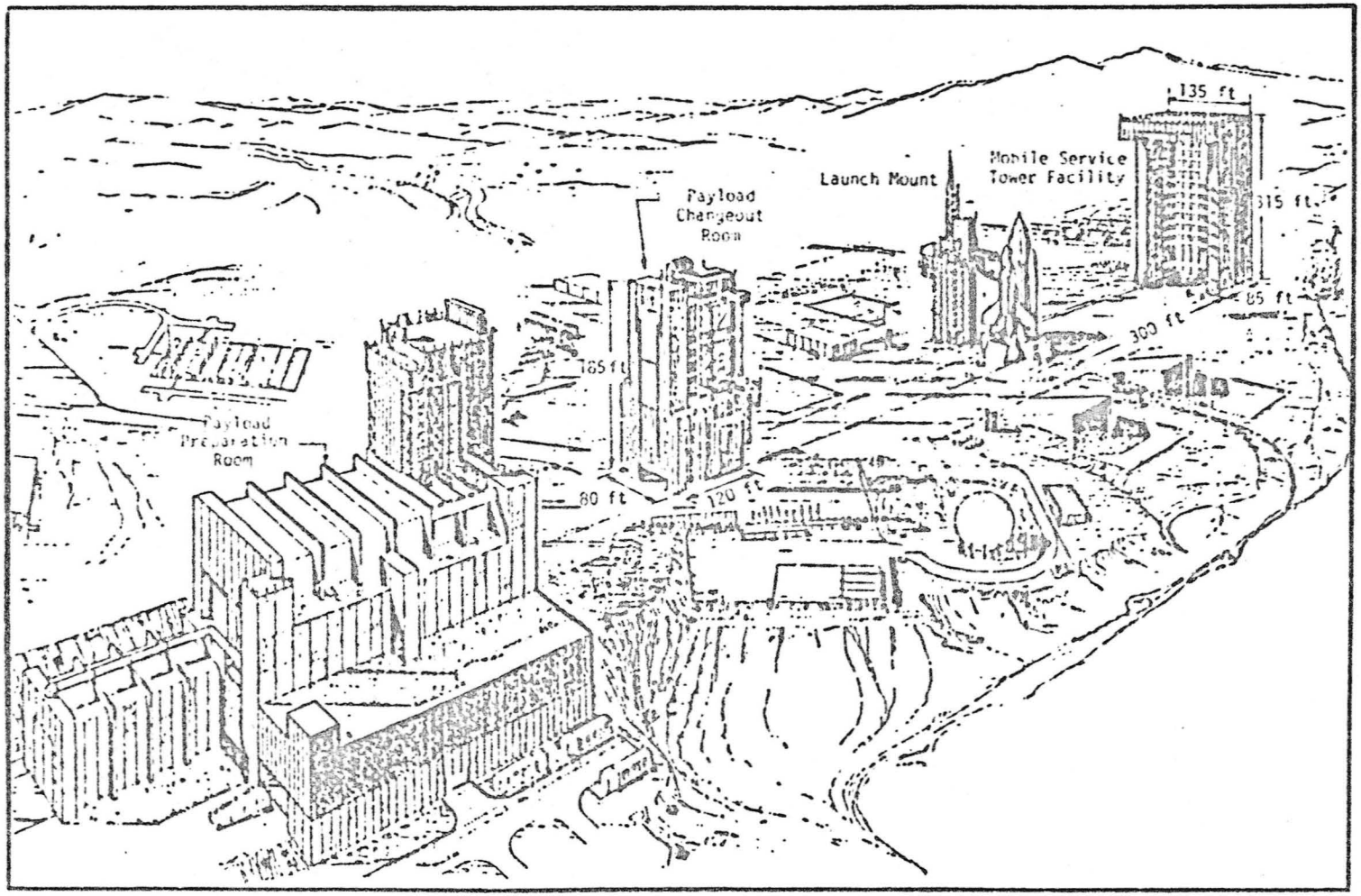

Figure 4.5. Launch site facility.

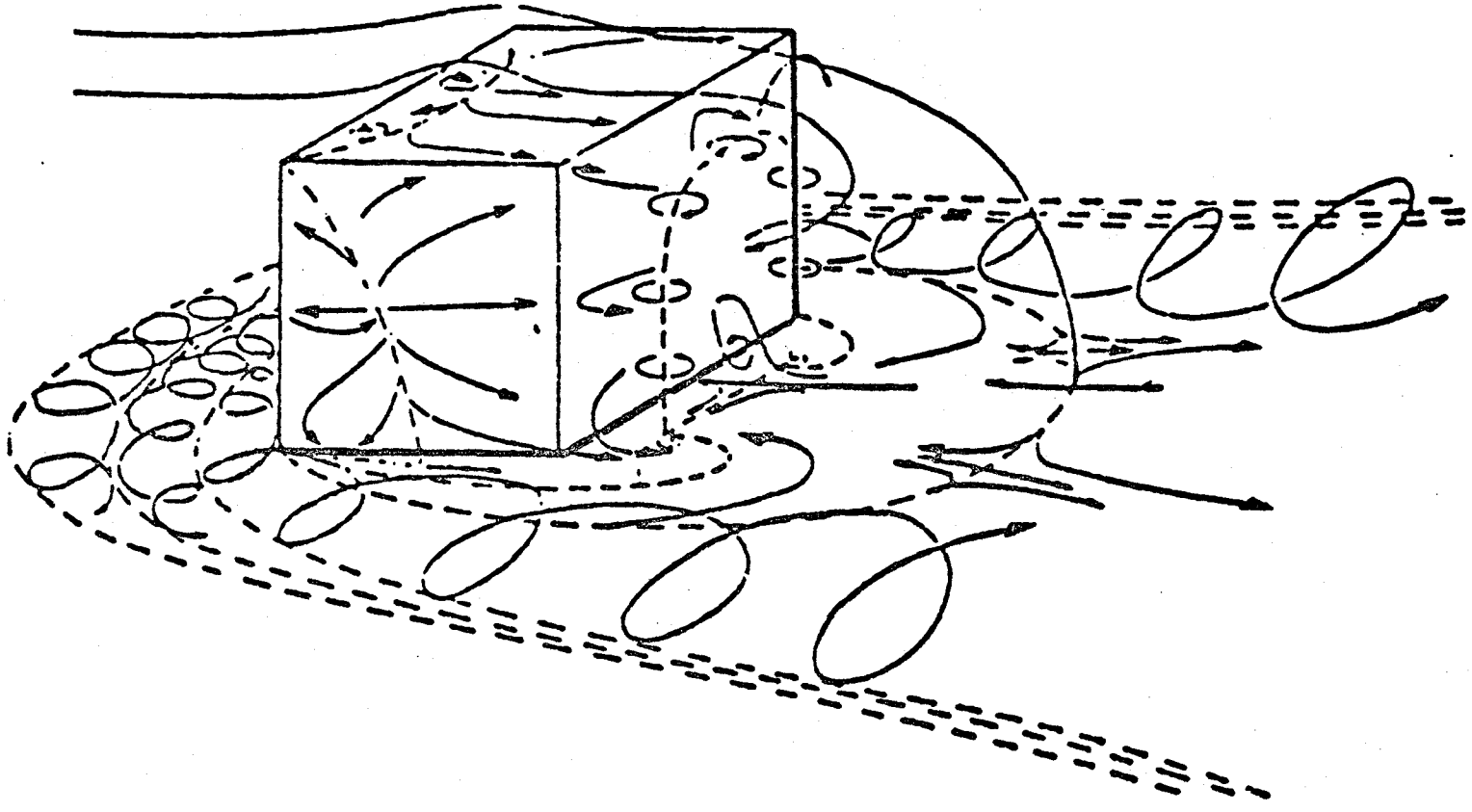

Figure 4.6. Flow pattern around a rectangular block with reattachment of the free shear flow (Woo et al. 1977).

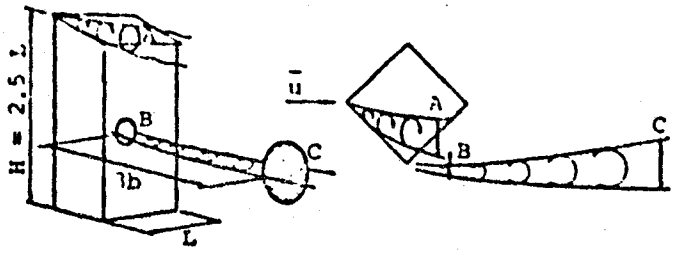

Schematic Showing Sections where Pressure Pulsations were Measured

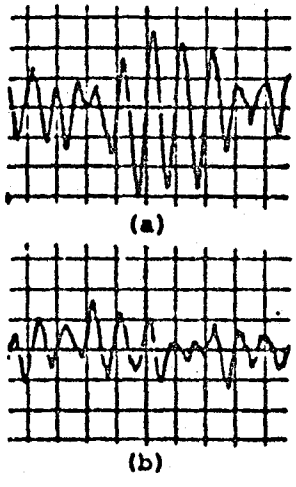

Oscillograms of Pressure Pulsations behind a Prismatic Model with a Sloping Roof. Each Horizontal Division--20 Milliseconds. Each Vertical Division--0.20 mm Hg. $\rho\bar{u}_\infty^2/2$ - 0.60 mm Hg.
(a) Region A (b) Region B

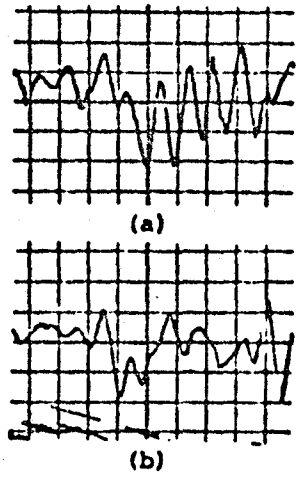

Oscillograms of Pressure Pulsations in Region C. Each Horizontal Division--20 Milliseconds. Each Vertical Division--0.20 mm Hg. $\rho\bar{u}_\infty^2/2$ - 0.60 mm Hg.
(a) Sloping Roof (b) Flat Roof

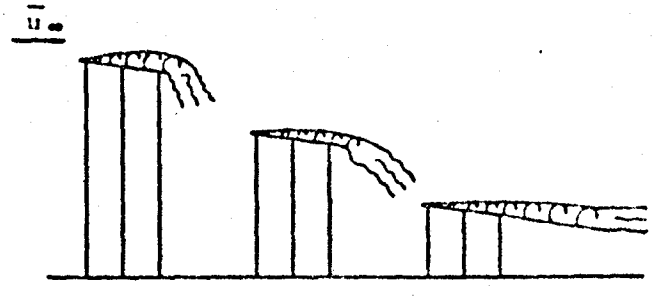

Schematic Showing Influence of Building Height on a Conical Vortex

Figure 4.7. Vortices generated on the leading edges of building models (Ostrowski et al. 1967).

whereas the inside flow is usually highly turbulent due to the interference effects from other flow regions. The turbulence is particularly high after vortex bursting.

Figure 4.8 shows the physical phenomenon of vortices shed by Jan Mayen Island. Therefore, vortices shed by the natural and man-made terrain features around VAFB (SLC-6) can have significant intensity to affect the STS launch to some extent.

4.3 Wakes

The separation region, which is also referred to as the wake behind a bluff surface feature, is a region of high turbulence. The extent of this region depends on the geometry of the obstacle and on the nature of the upstream flow.

In discussing the wake, one must consider the distinction between a momentum wake (normal wake) and a vortex wake (Hansen and Cermak 1975). Both wakes interact and form the overall wake which creates disturbance in the flow field downstream of a protrusion. The degree to which each wake dominates the flow field is quite different, depending on the geometry and orientation of the body. Data presented by Lemburg (1973) indicate that the mean velocity wake behind a block geometry with flow perpendicular to one of the plane surfaces extends to a distance downstream of 10 to 15 block heights. However, the wake can extend to 50 to 100 block heights, or radii, downstream when the wind approaches a rectangular geometry at other than perpendicular to a plane surface, or flows around circular cylinder or hemisphere blocks. This observed effect can be contributed to the dominance of the momentum or the vortex wake. A two-dimensional body having the wind approaching perpendicular to the long axis is the only geometry which has a fully momentum-produced wake. As the width of the protrusion becomes finite, the end effects cause the formation of vortices.

Figure 4.9 shows the dimensionless extent of the separated flow zone, x_r/H, as a function of the aspect ratio, L/H, for blocks with

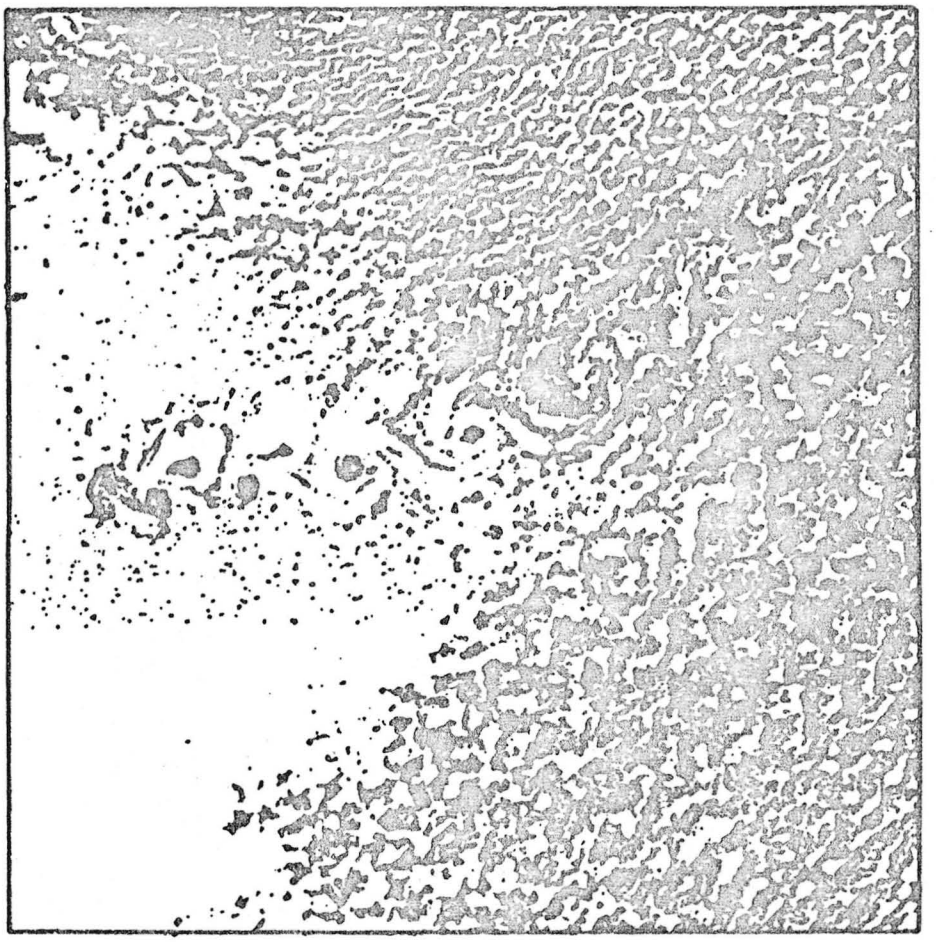

Figure 4.8. Satellite photo of vortices shed by Jan Mayen Island (Arctic Ocean) (Simiu and Scanlan 1978).

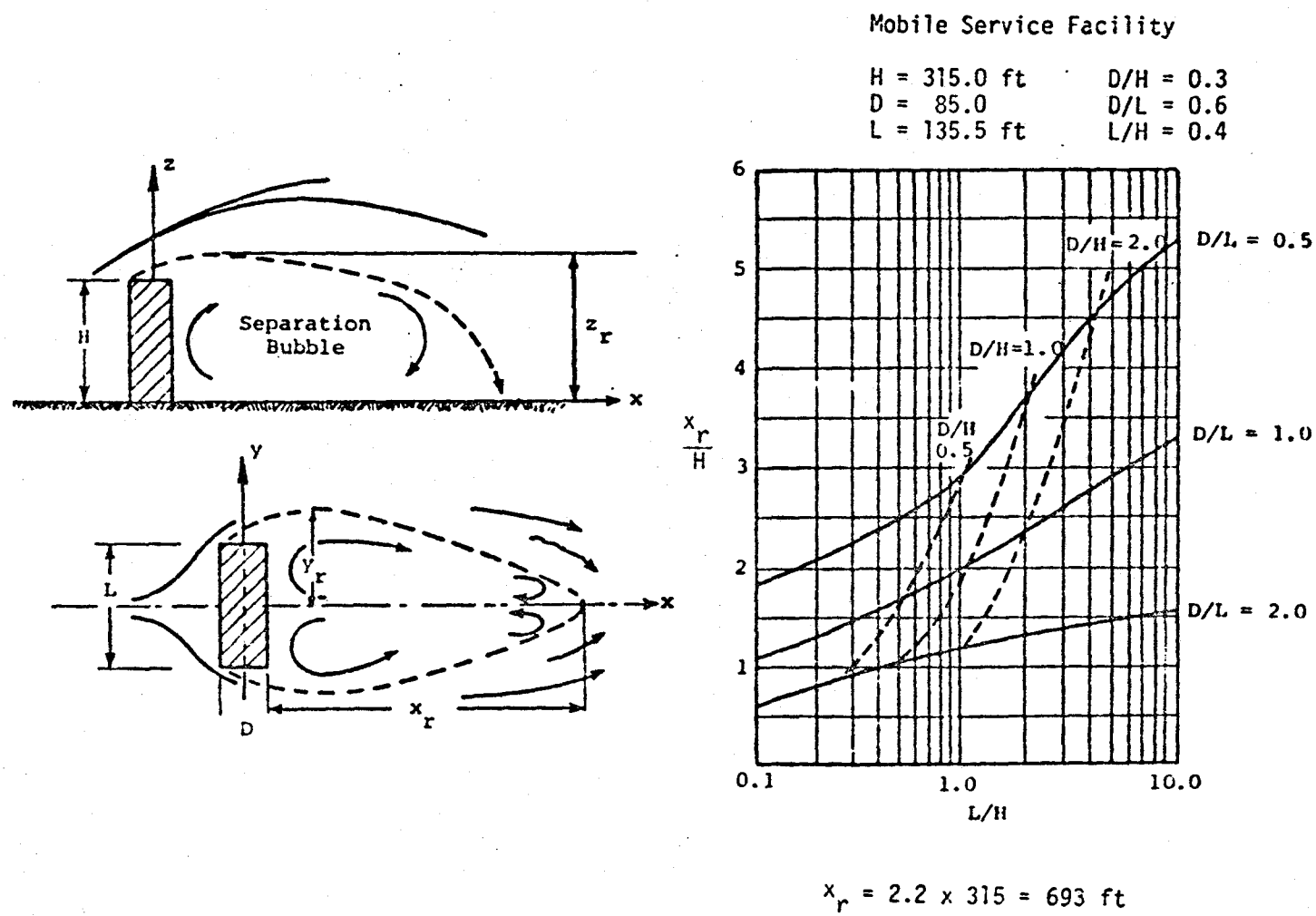

$x_r = 2.2 \times 315 = 693$ ft

Figure 4.9. Wake geometries behind a three-dimensional bluff body.

different ratios of D/L (Leutheusser and Baines 1967). The nomenclature is defined in Figure 4.9 where H is the height, L is the length, D is the depth, and x_r is the distance where the flow reattaches to the surface behind the block. The data are from wind tunnel measurements for a simulated atmospheric wind speed profile approaching perpendicular to the front face of the block. The region of recirculating flow is observed to increase with decreasing values of D/L. Thus, long thin structures or terrain features perpendicular to the prevailing wind direction produce the larger separated flow regions.

Consider the man-made buildings around the VAFB (SLC-6) launch site (Figure 4.5) again. The corresponding reattachment distance, x_r, of the mobile service tower facility can be interpolated from Figure 4.9 as being 693 ft (211.2 m) approximately. The launch pad is unfortunately located at about the center of the wake induced by the mobile service tower.

Figures 4.10 and 4.11 compare the lateral velocity profiles behind a block perpendicular to the flow and the same block at a 47° angle to the flow. Comparison of the two figures shows dramatically the difference between the two wakes. The wake behind the block with a plane surface perpendicular to the flow is a more symmetric and less persistent wake, whereas the wake behind the block oblique to the flow persists well downstream, continuing beyond 80 building heights. $\bar{u}_0(z)$ is the undisturbed wind speed perpendicular to the windward face in the x-direction and is measured at the same height z as the locally disturbed wind speed $\bar{u}(z)$. $\bar{u}_\infty$ is the freestream velocity measured at approximately z = 10 H.

By using the results shown in Figures 4.10 and 4.11, the conceptual wake patterns behind the mobile service tower of the corresponding cases in these two figures are deduced and shown on the right side of each figure. Wind loading on space shuttle launching in the wake region is preliminarily estimated in Section 6.0.

An orographic measurement program using the NASA B-57B aircraft was conducted in the Denver-Boulder, Colorado, area in 1984 by the Ames/Dryden Flight Research Facility of Edwards, California, and the Marshall

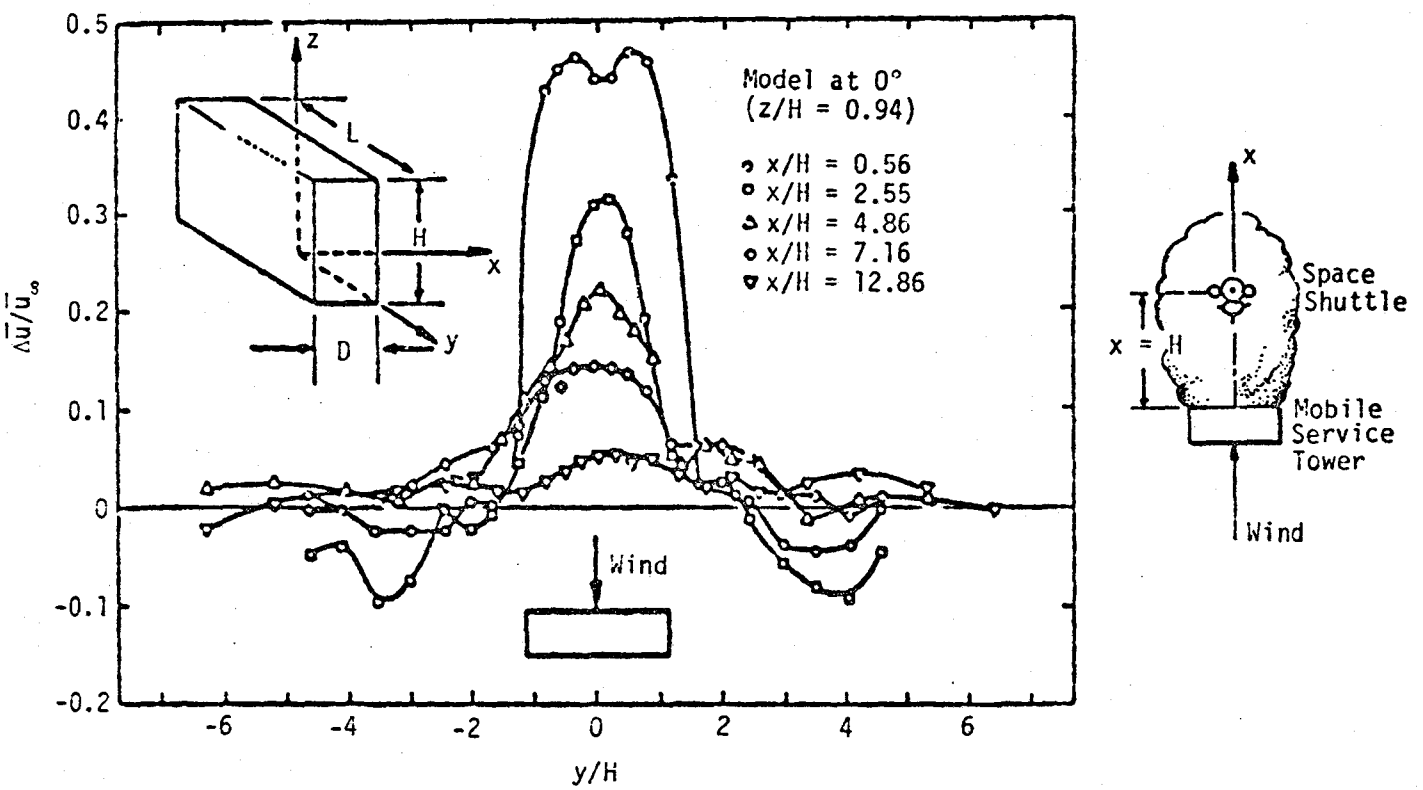

Figure 4.10. Lateral profiles of mean velocity deficit in the wake of a block at 0° (Woo et al. 1977).

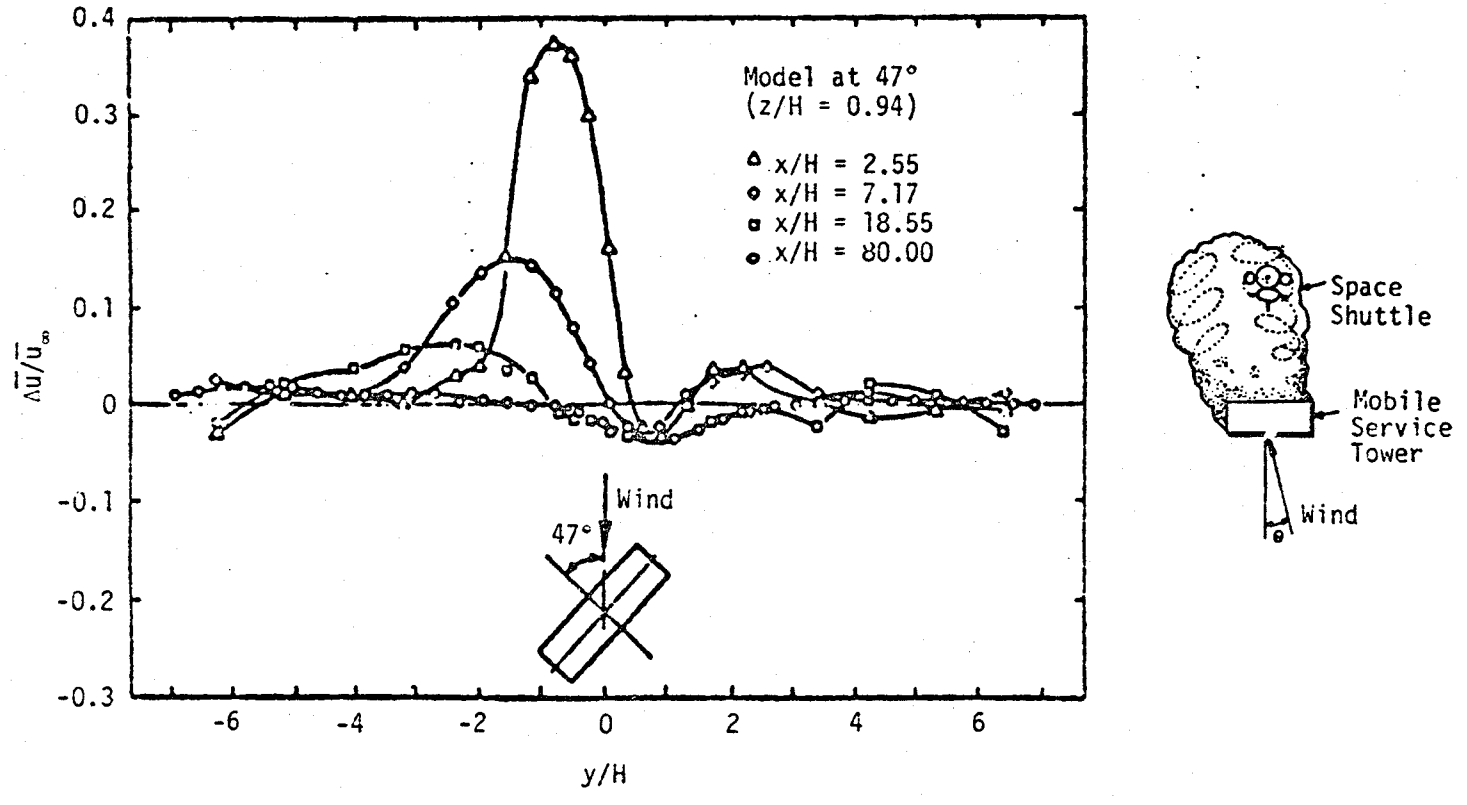

Figure 4.11. Lateral profiles of mean velocity deficit in the wake of a block at 47° (Woo et al. 1977).

Space Flight Center of Huntsville, Alabama. Preliminary analysis of the data from Flight 60 of this program are shown in Figures 4.12 through 4.14. These data were obtained in the lee (wake area) of the Rocky Mountains just north of Denver and over Boulder, Colorado. By inspecting the wind field of the wake region, as shown in these figures, one can easily see that the influence of the wake due to natural and man-made features in the VAFB (SLC-6) launch area could be very significant to the STS launches.

4.4 Mountain-Valley Wind

Mountain and valley breezes result from the diurnal temperature variation in valleys, which causes a pressure gradient from the plain to the valley during the daytime (the valley breeze) and a reverse gradient at night (a mountain breeze). Defant (1951) has summarized the basic theory in observations of mountain-valley flows. A schematic illustration of the normal diurnal variation of the circulation system in the valley is shown in Figure 4.15. The black arrows show mountain or valley breeze, and white arrows show up- or down-slope wind and its associated circulation.

The actual state of the mountain and valley breezes varies according to factors such as topographical conditions, seasonal change of the height of the sun, duration of daytime and nighttime hours, vegetation, and surface conditions. Many parameters affecting the wind characteristics in a valley along with the variability of these parameters from valley to valley make it nearly impossible to draw specific conclusions concerning effects of the various parameters which will remain valid for all valleys.

Generally speaking, long deep valleys with floor slope greater than 0.1 have valley and mountain winds averaging from 6 to 16 knots (3 to 8 m/s), and slope winds averaging from 4 to 8 knots (2 to 4 m/s). Investigation of the topograph VAFB (SLC-6) launch area has been carried out. A broad shallow valley along the direction from southeast to northwest has a floor slope less than 0.07. Therefore, mountain-valley winds around the VAFB (SLC-6) site are not as important as the others previously mentioned.

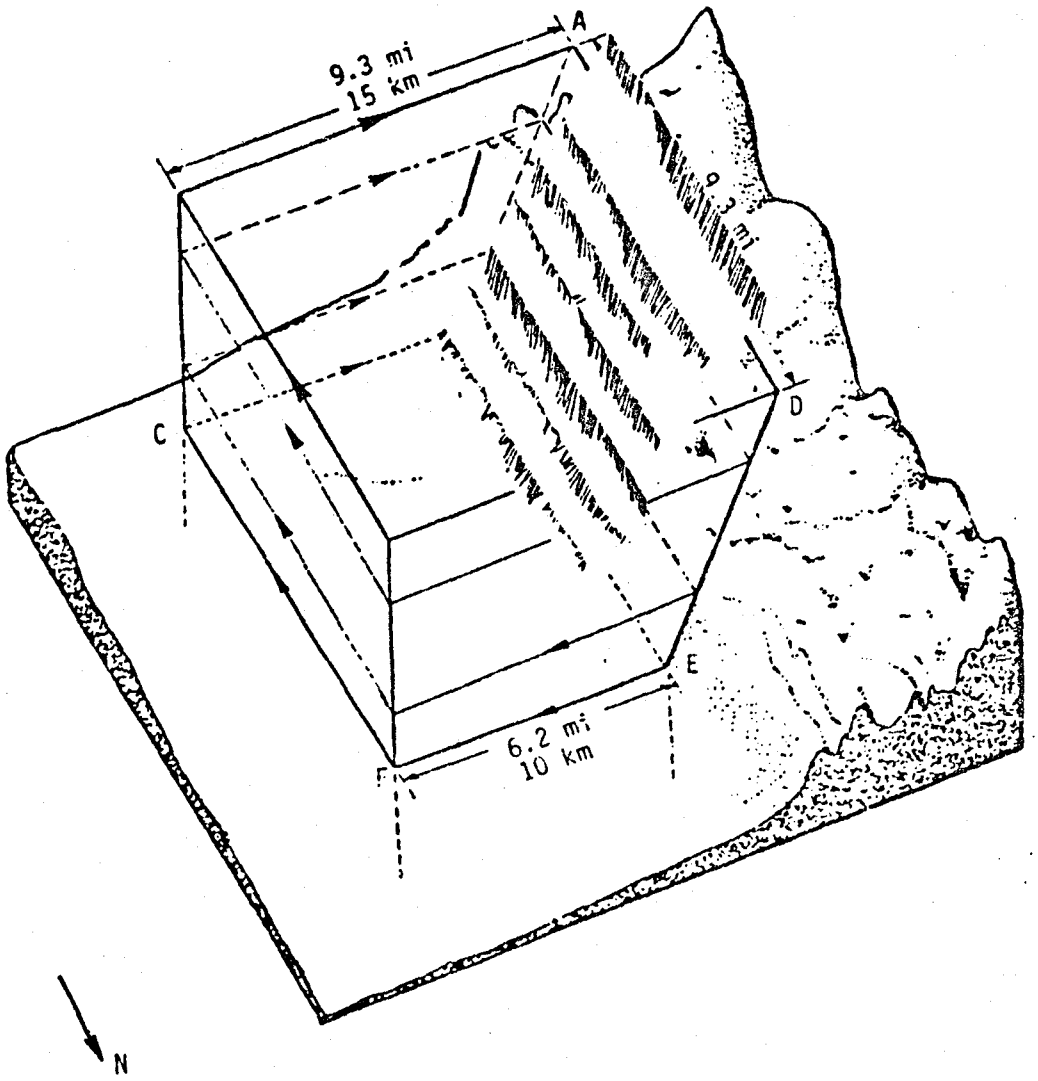

Figure 4.12. Horizontal wind field recorded on orographic effects Flight 60.

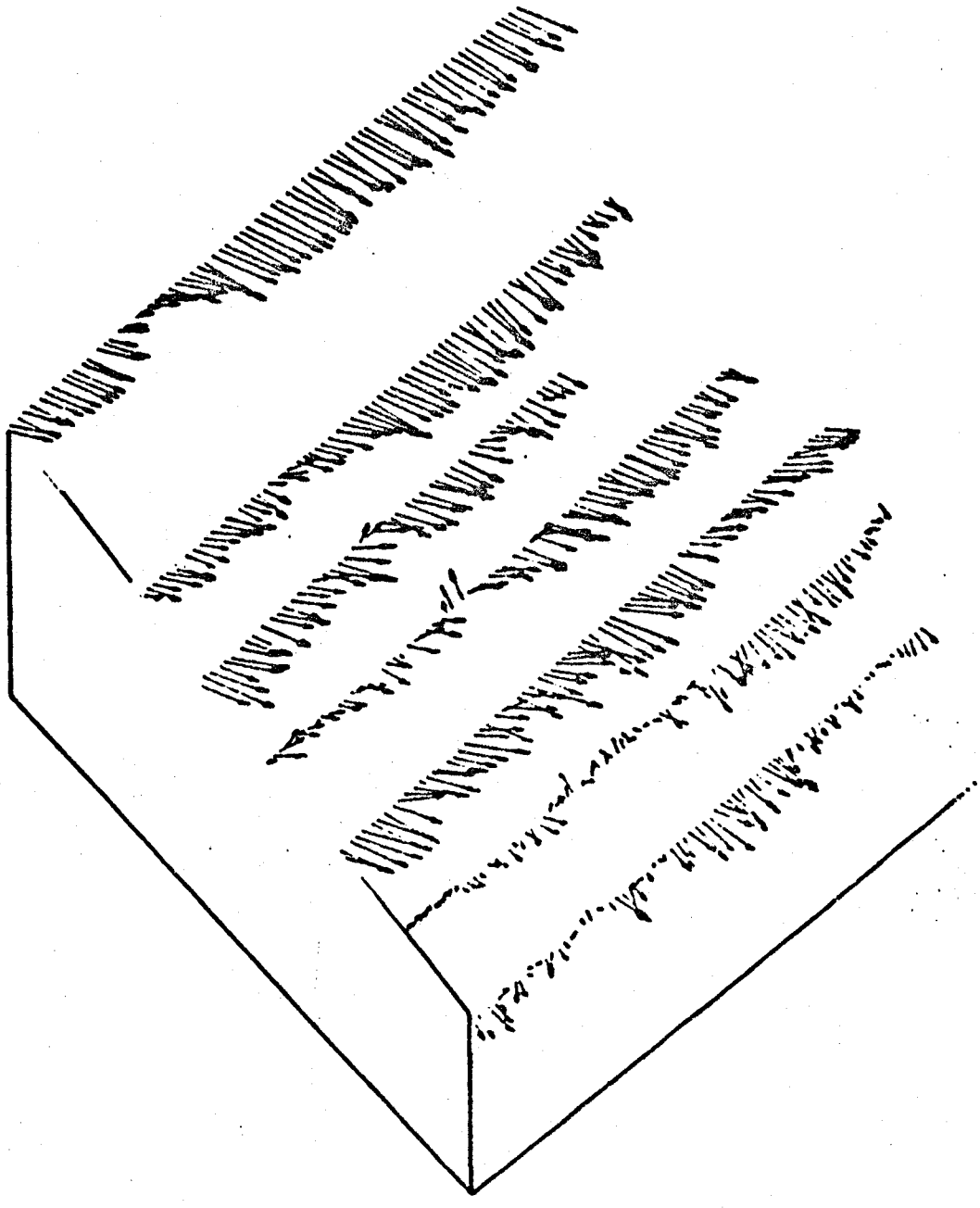

Figure 4.13. Horizontal wind vector at different levels along mountain side.

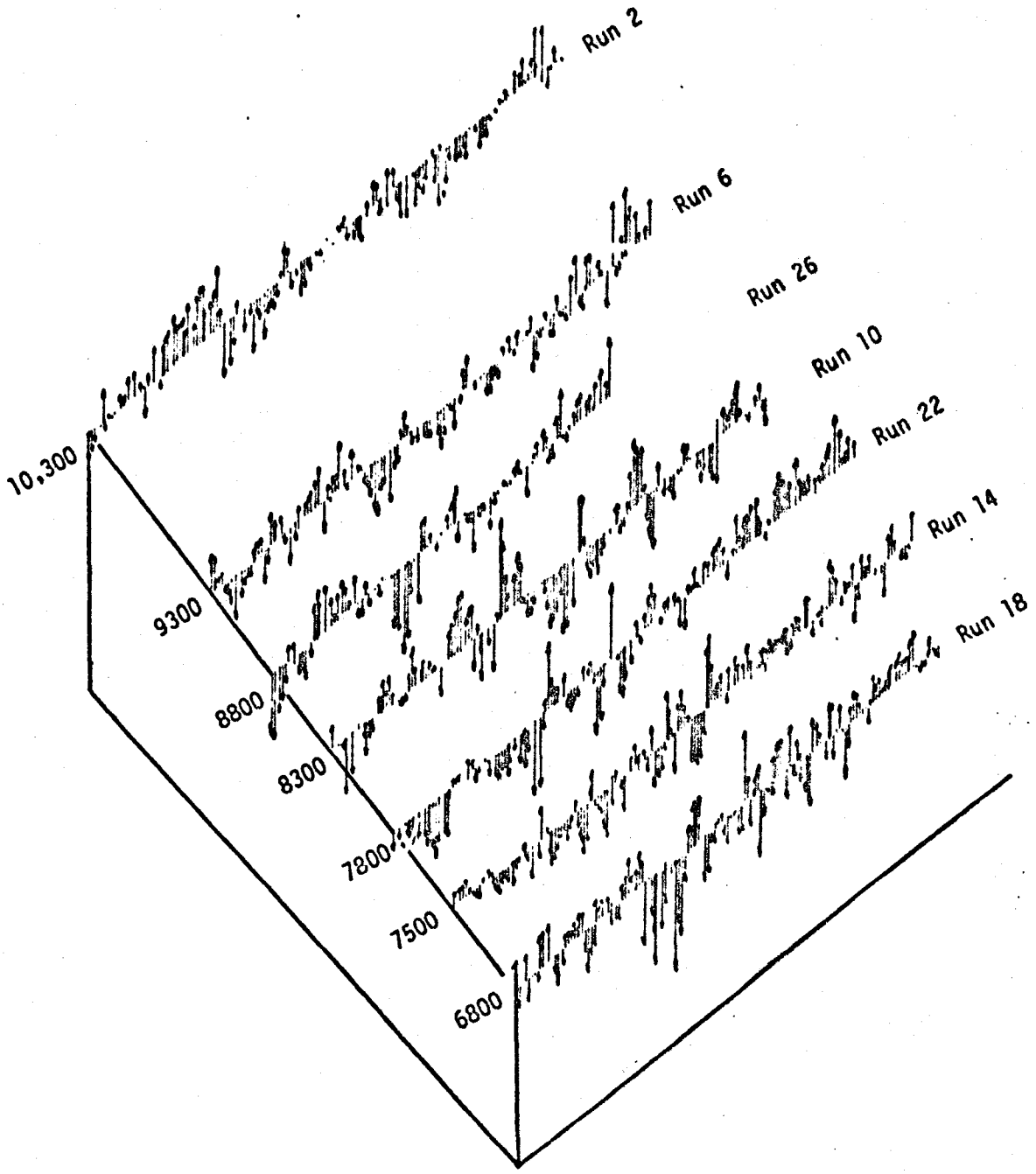

Figure 4.14. Vertical wind vector at different levels along mountain side.

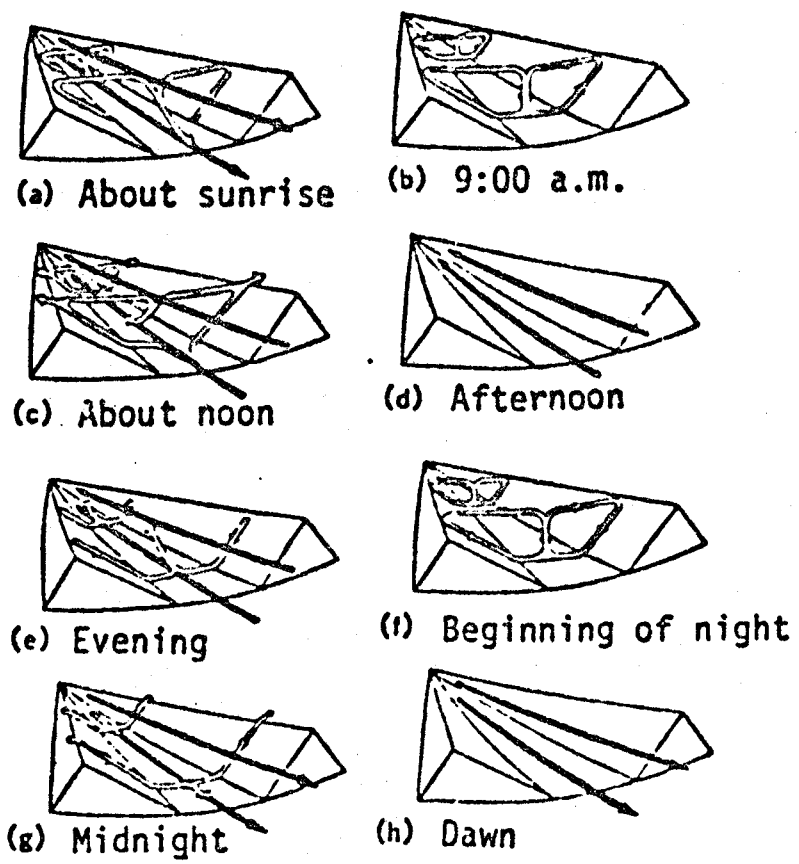

Figure 4.15. Schematic illustration of the normal variations of the air currents in a valley.

5.0 FLOW PATTERN OVER THE VAFB SLC-6

Vertical cross-sectional flow patterns for eight directions over the natural terrain passing through the center of the VAFB (SLC-6) launch site are approximately discussed in this section. General characteristics of flow fields around several isolated terrain features have been described in Section 4.0. The concept of a two-dimensional flow field is useful because it represents a limiting condition for which a great deal of analytical and experimental data are reported. Therefore, the criterion for flow separation over two-dimensional triangular hills (Figure 4.3) has been applied to predicting the flow pattern of each cross section. As mentioned earlier, the extent of the separation region which is the region of high turbulence depends on the geometry of the obstacle magnitude and on the nature of the upstream flow.

Figure 5.1 shows the flow patterns in cross sections at directions of:

a. NW to SE at 135° from north (clockwise +)

b. Reverse direction of (a)

c. NW to SE at 112.5° from north

d. Reverse direction of (c)

e. W to E at 90° from north

f. Reverse direction of (e)

g. SW to NE at 67.5° from north

h. Reverse direction of (g)

i. SW to NE at 45° from north

j. Reverse direction of (i)

k. SW to NE at 22.5° from north

l. Reverse direction of (k)

m. S to N at 0° from north

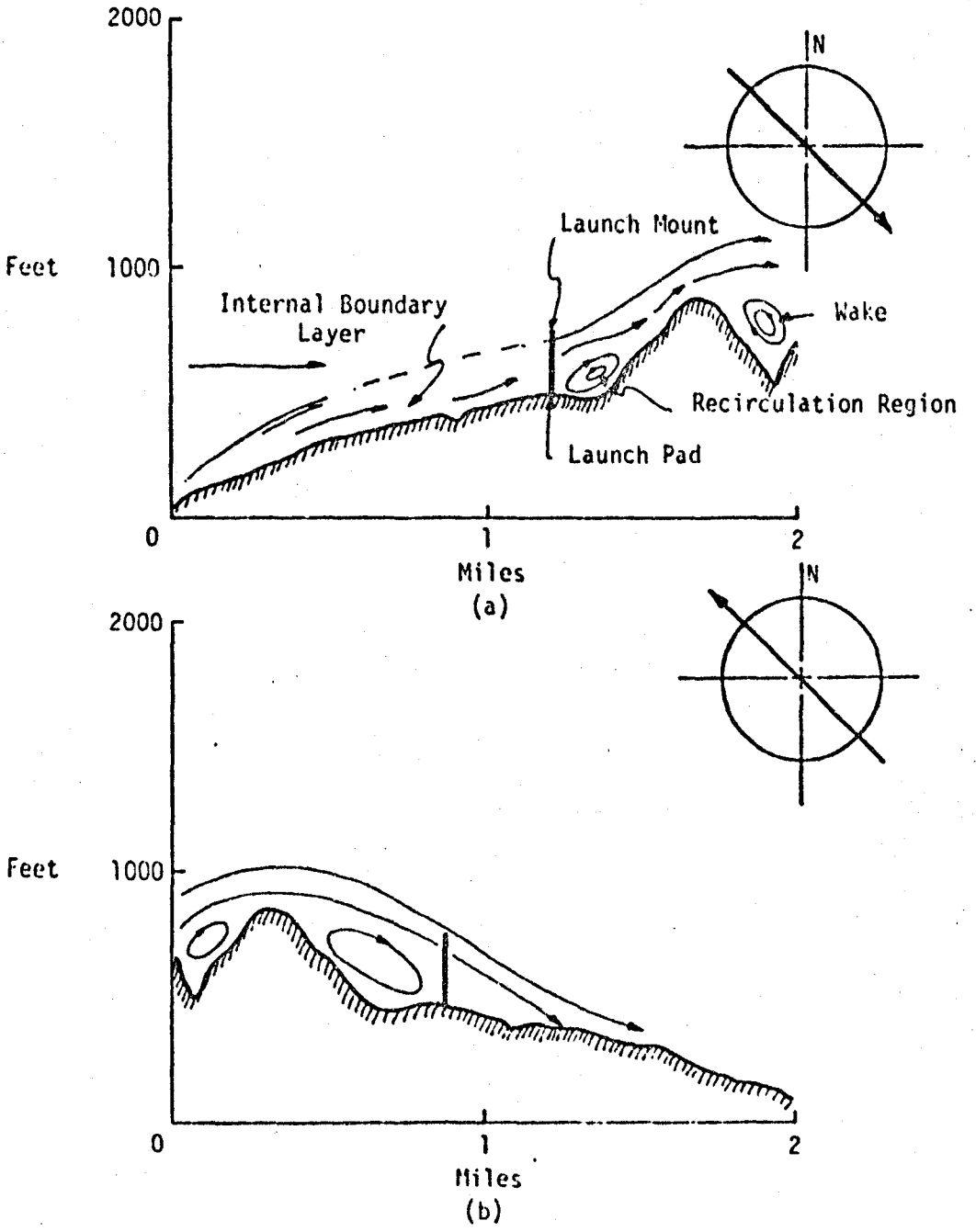

Figure 5.1. Flow pattern over the VAFB (SLC-6) launch area.

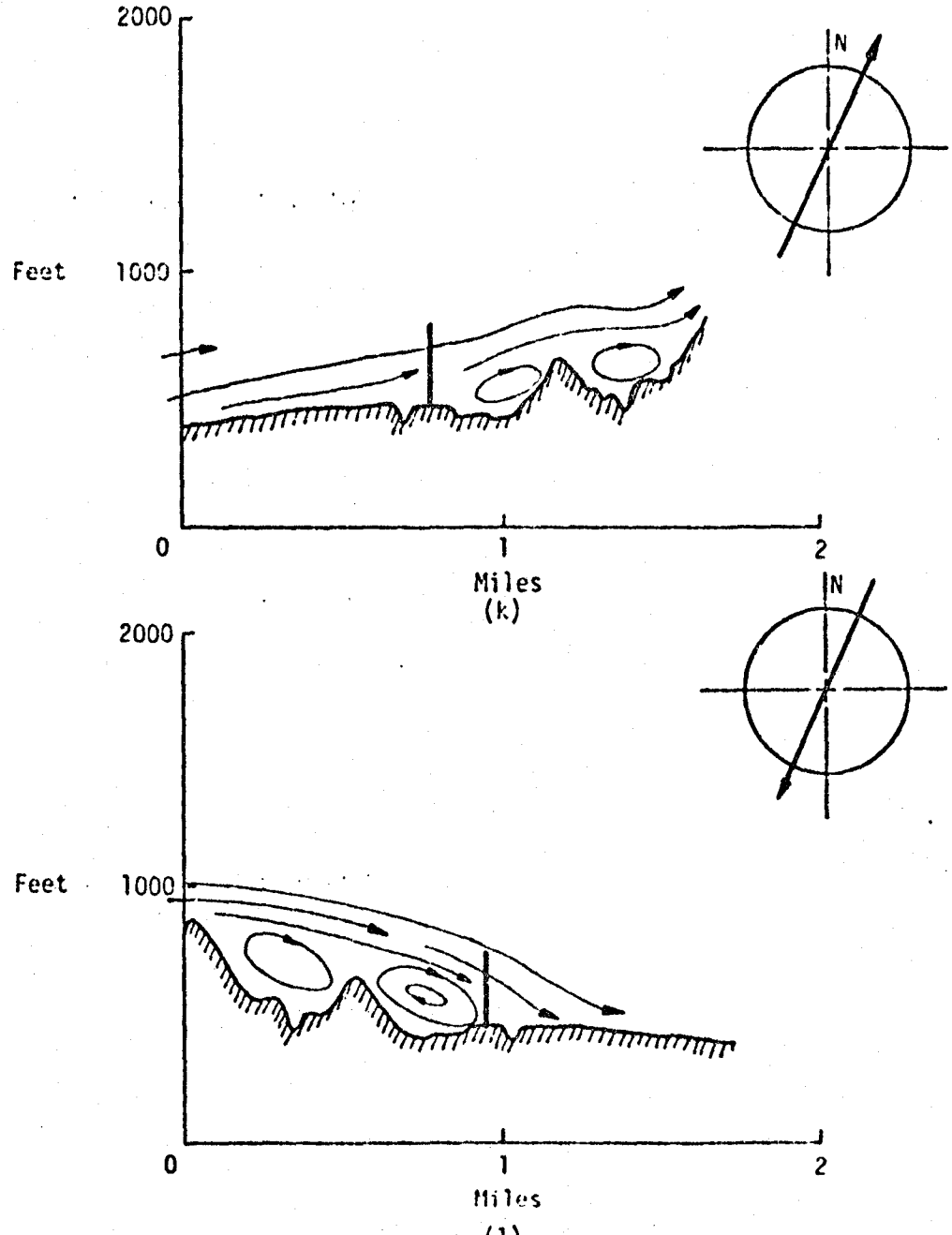

Figure 5.1. (continued).

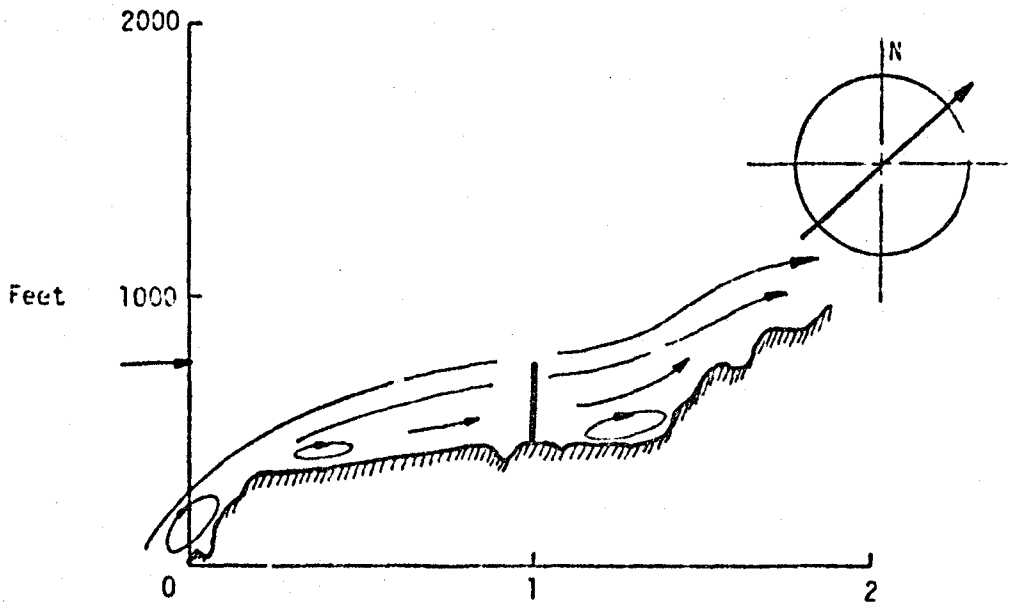

(i)

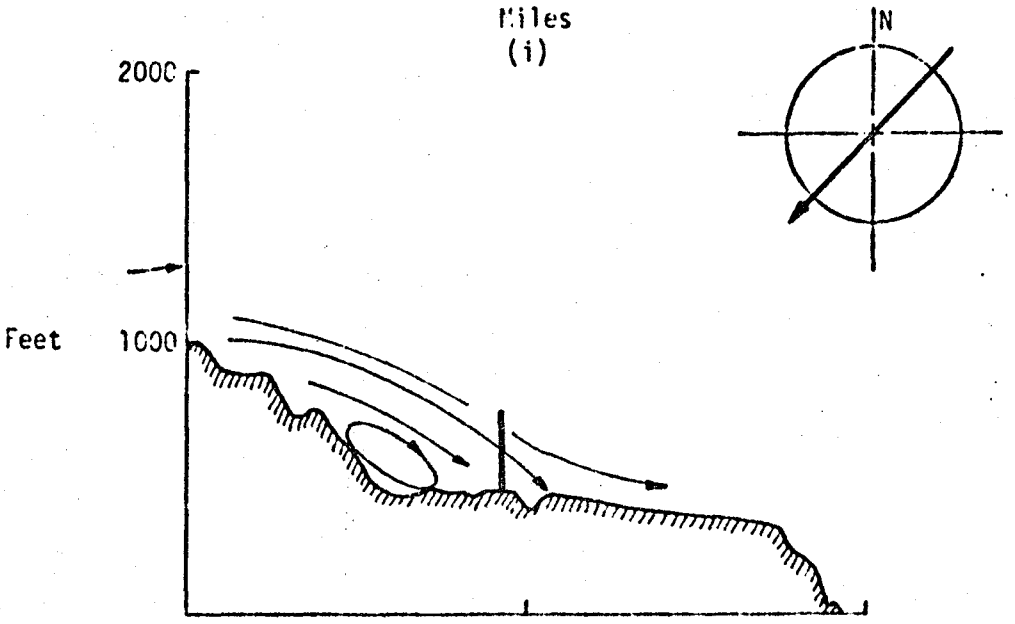

(j)

Figure 5.1. (continued).

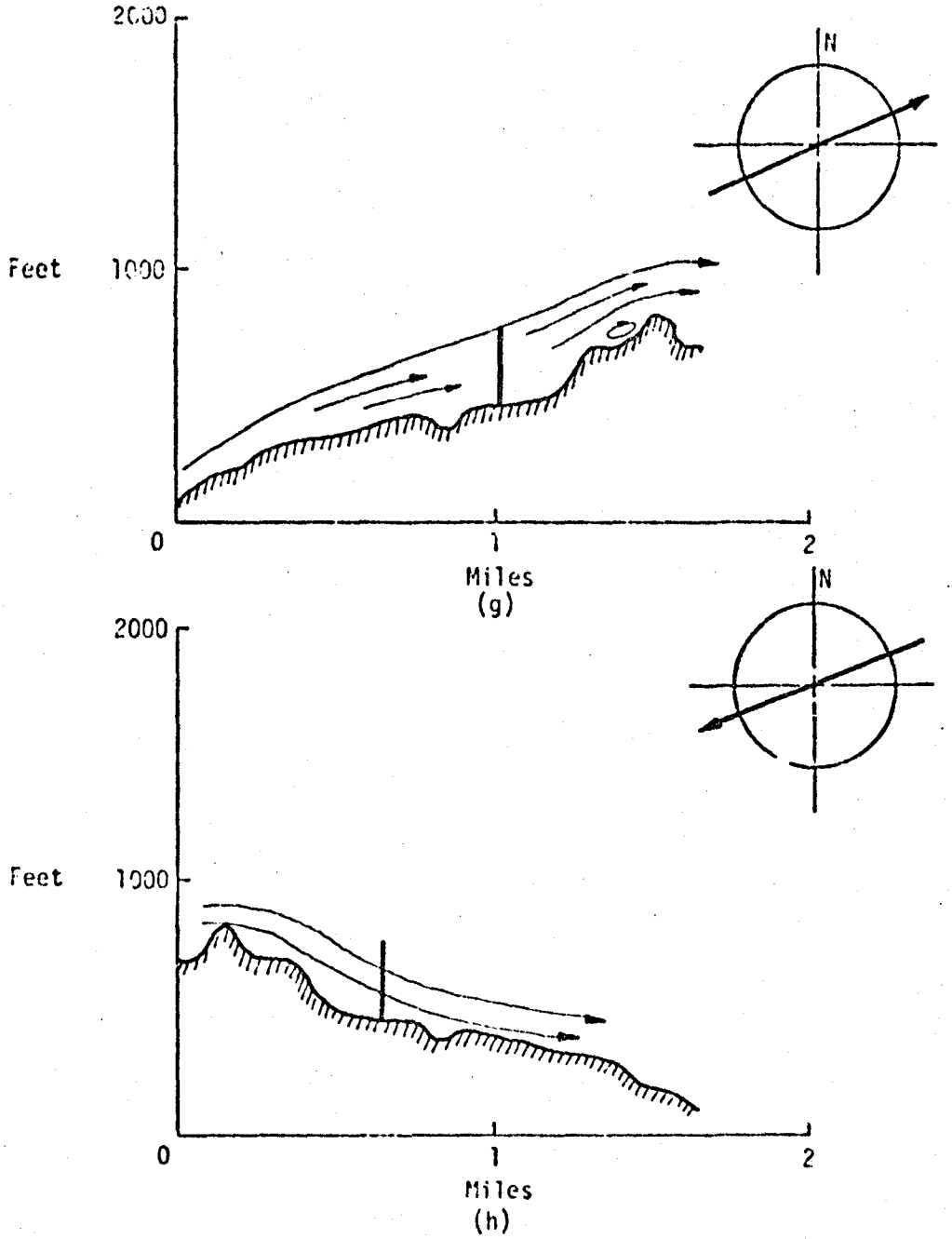

Figure 5.1. (continued).

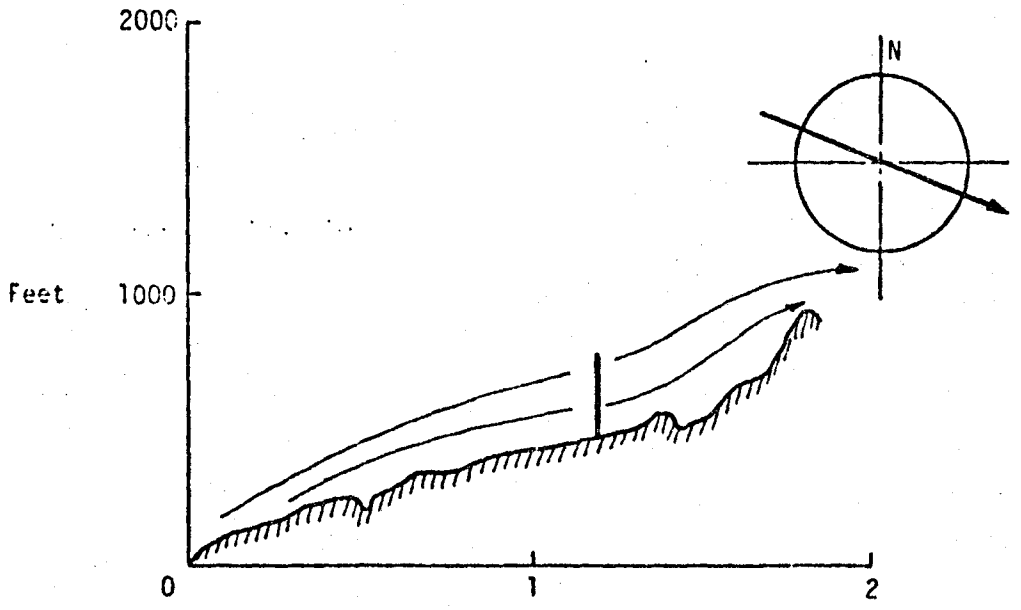

(c)

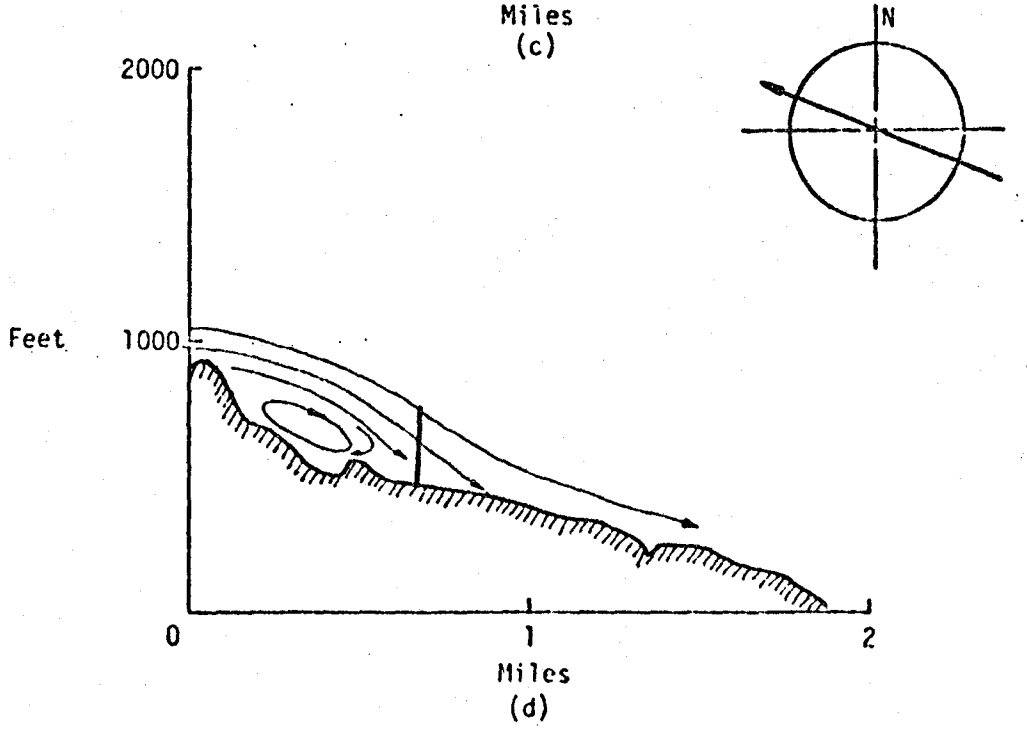

(d)

Figure 5.1. (continued).

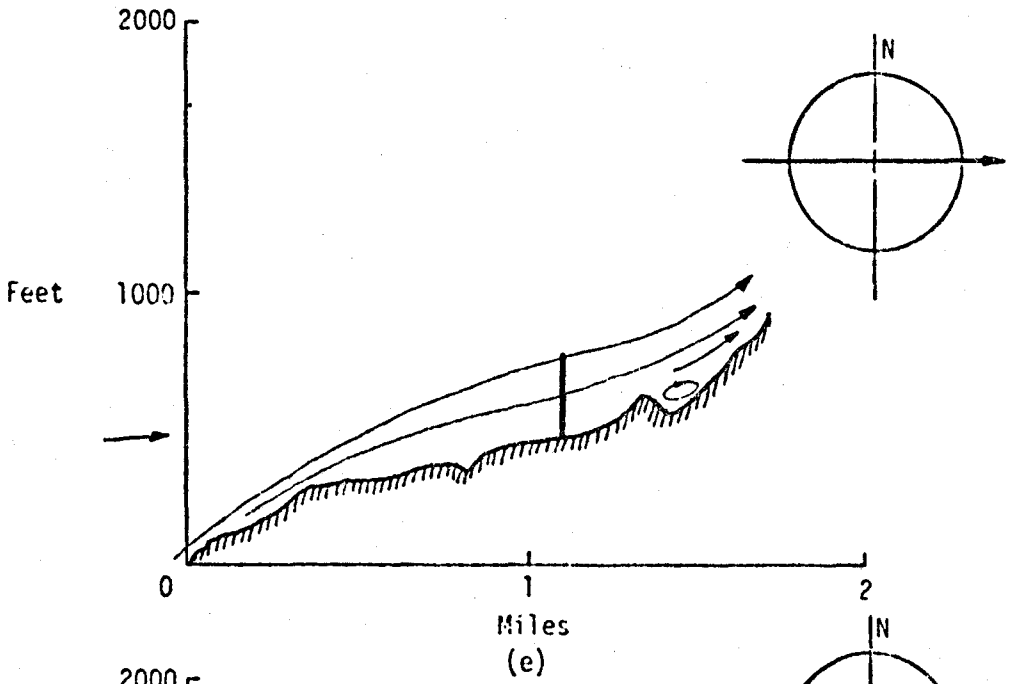

(e)

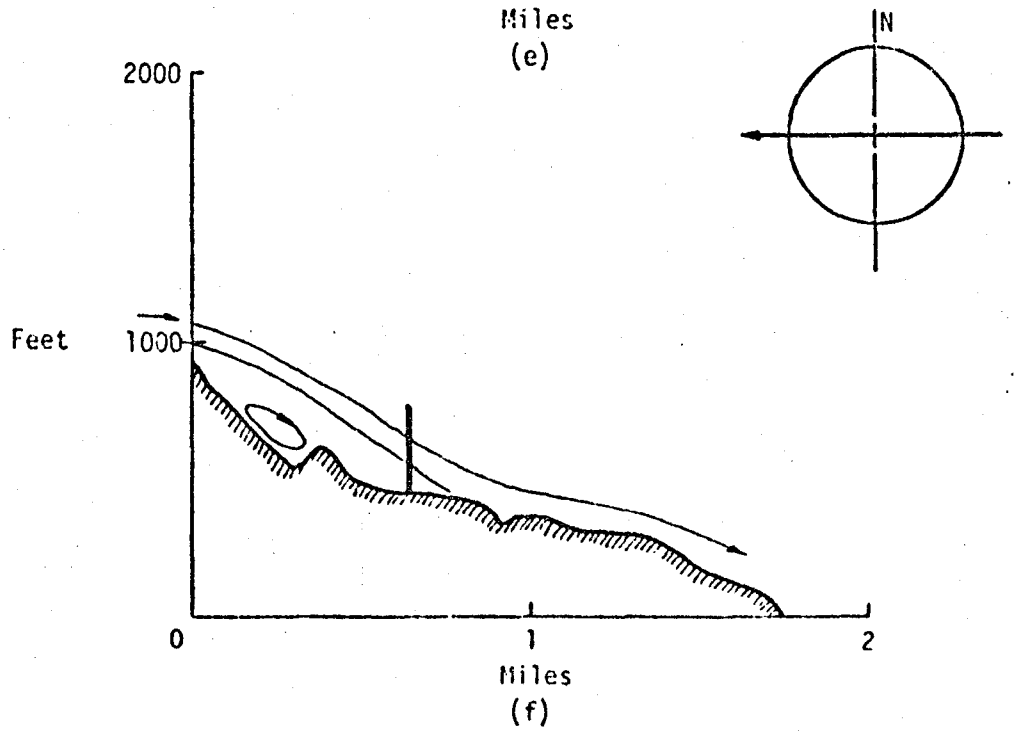

(f)

Figure 5.1. (continued).

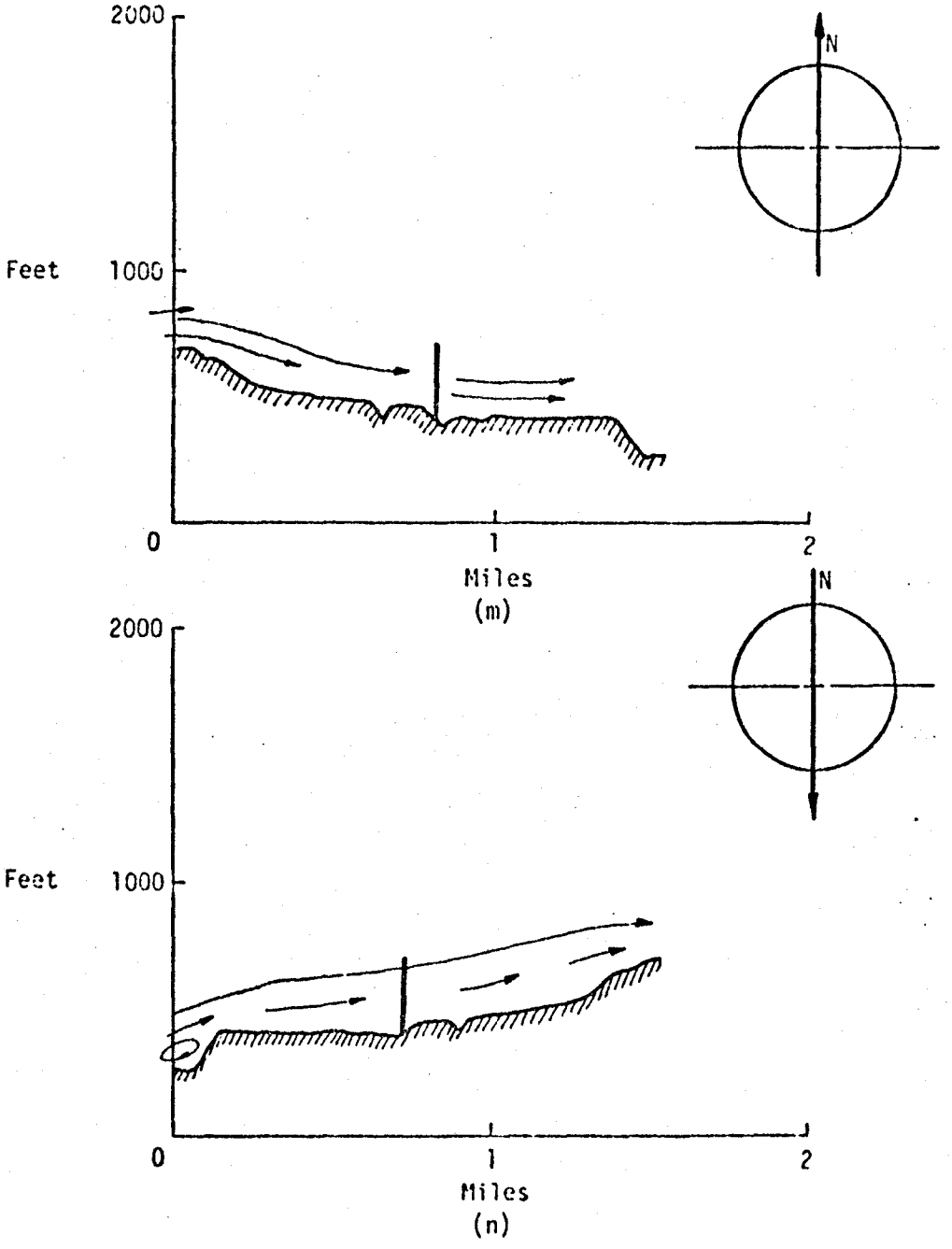

Figure 5.1. (continued).

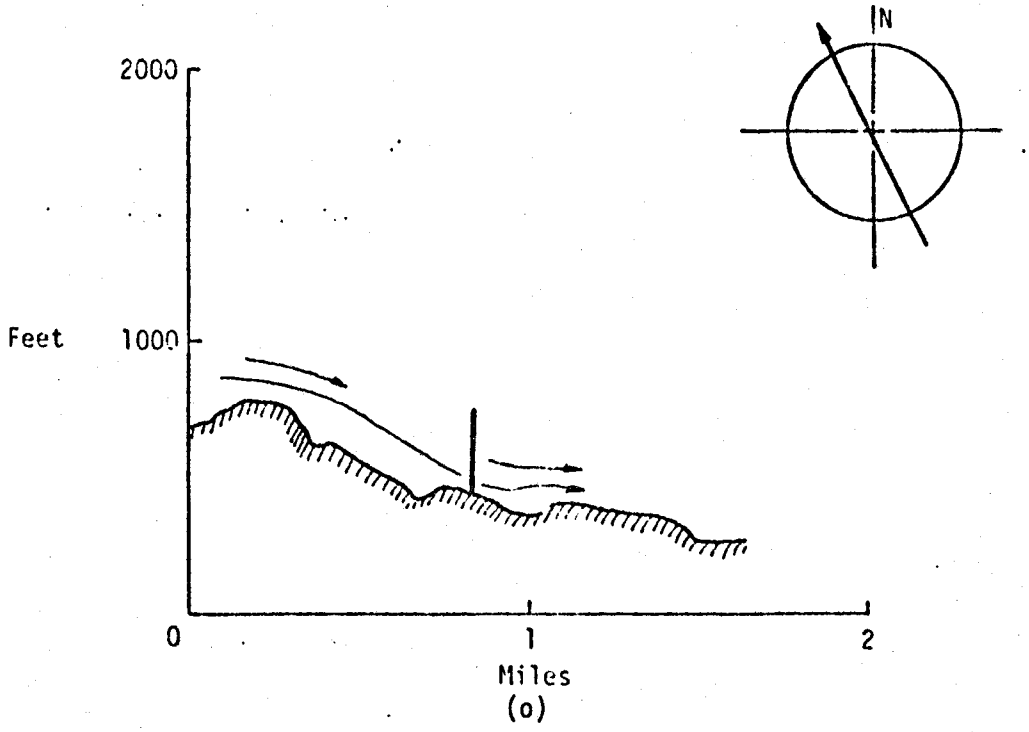

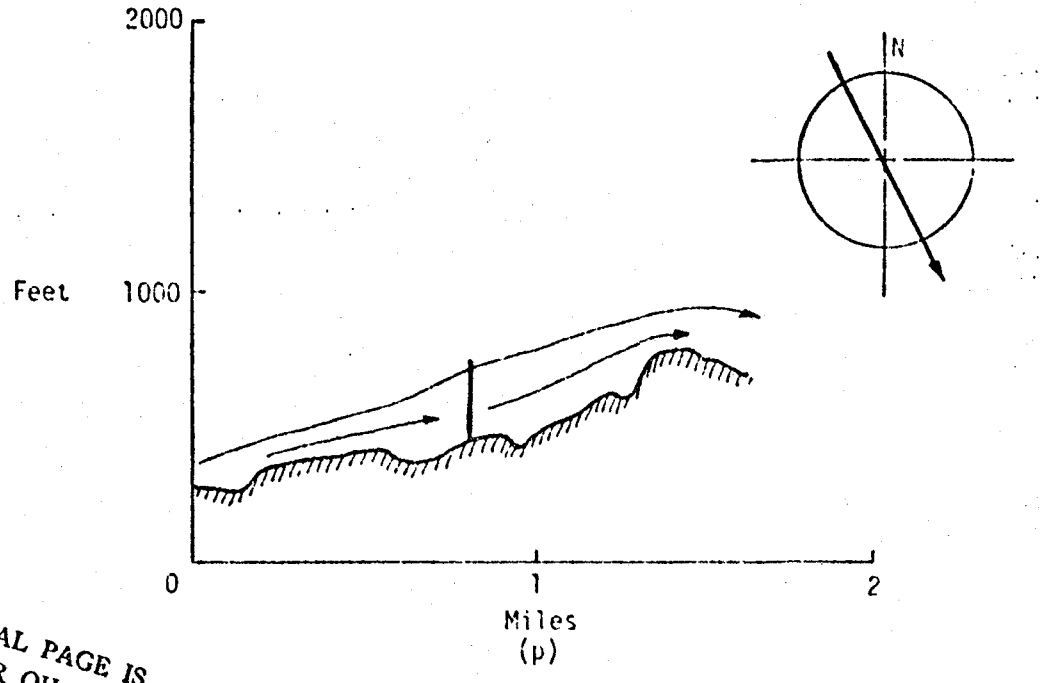

Figure 5.1. (continued).

n. Reverse direction of (m)

o. SE to NW at -22.5° from north

p. Reverse direction of (o)

The prevailing wind direction is shown at the upper right-hand corner of each figure. The predicted flow pattern along the terrain surface is also plotted in each figure. Separation region always occurs to the downstream and sometimes to the upstream of a hill. Figure 5.1a shows that wind flows from northwest direction (onshore wind) which is the predominant wind direction around VAFB (SLC-6) launch site. The launch mount which has a height of 300 feet is plotted above the terrain surface (see Figure 4.5). As shown in Figure 5.1a, there is a hill-like block just behind the launch pad. In addition to the wake occurring to the downwind of the hill, a big recirculation region also occurs to the windward side. The launch mount and space shuttle are initially immersed in the internal boundary layer dominantly due to the roughness of the terrain surface. Thus, the big recirculation region at the windward side of the hill will strongly affect the space shuttle launch.

Similarly, considering that wind is blowing through the same cross section in the inverse direction from southeast to northwest, and is strong enough, the downstream wake region at the downwind site of the hill will significantly influence the STS launch. All eight cross sections corresponding to 16 cases have been investigated in this report. Most of the cases have recirculation flow effects around the launch station.

6.0 PRELIMINARY ESTIMATE OF THE MAGNITUDE OF WIND LOADING ON STS

The nature of the flow over natural and man-made terrain features has been reviewed in the last few sections. As mentioned earlier, the wind loading on the space shuttle while standing on the launch pad and during initial liftoff is very complex. Consider the flow pattern around a rectangular block which has the same nomenclature as shown in Figure 4.10. Woo et al. (1977) measured velocities behind block-shaped bluff bodies of different aspect ratios, L/H. The aspect ratio is a measure of the blockage effect that the bluff body presents to the flow. Figure 6.1 indicates that the maximum wind speed occurs at z/H = 1.93 and x/H = 1.0. Figure 6.2 shows the results of the velocity measurement for the model of smaller aspect ratio (L/H = 2.44). A comparison of the results shown in Figures 6.1 and 6.2 indicates that:

1. Along the centerline of the flow field, the location of the maximum wind speed seems to be independent of the aspect ratio.

2. The maximum wind speed in the plane of symmetry through the flow field appears to fall between z/H = 1.93 and z/H = 3.75 at x/H = 1.0. The aspect ratio of the mobile service tower at VAFB (SLC-6) is about 0.4. The distance between the launch pad and the tower is almost equal to the height of the mobile service tower. Thus, wind bending load, which is induced by the mobile service tower, is acting on the space shuttle and is approximately estimated as shown in Figure 6.3.

The wind shear loading during the early stage of liftoff of the STS will have an influence, to some extent, on the controllability of the flight path direction. If the wind blows toward the mobile service tower at a certain angle rather than perpendicular to the building, the vortex shedded from the building will have a stronger effect on the launch. It is apparent that additional measurements and analyses are required to quantify the magnitude of these complex wind loads.

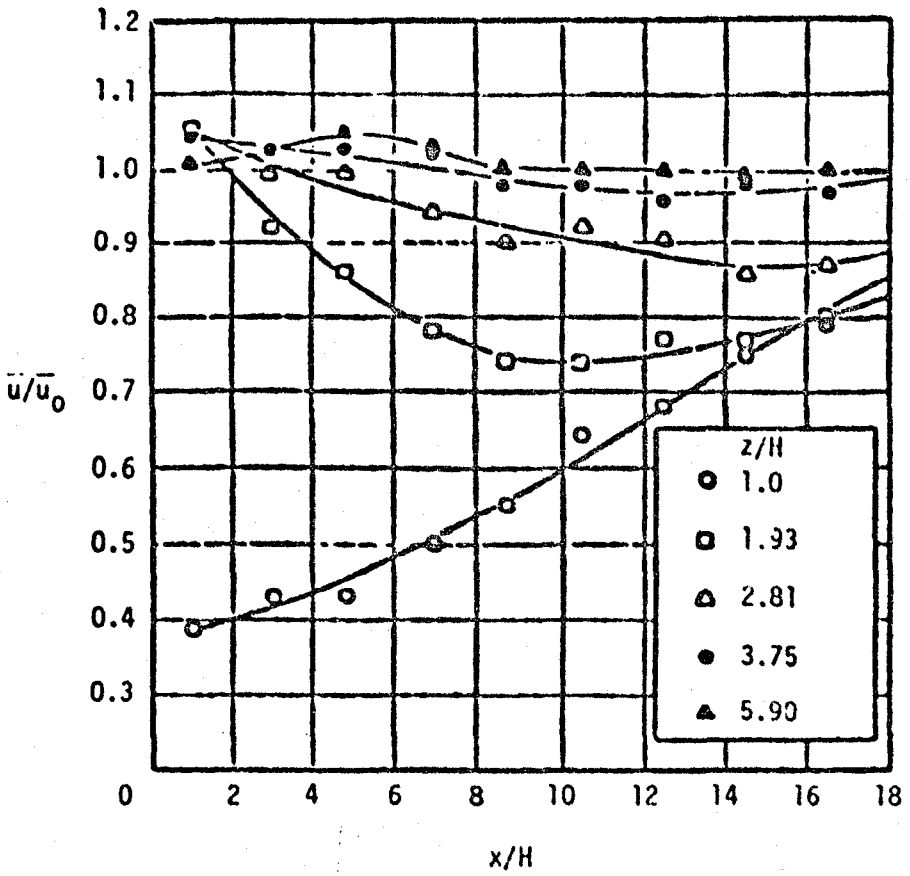

Figure 6.1. Velocity ratio at y/H = 0 for block aspect ratio = 8.37.

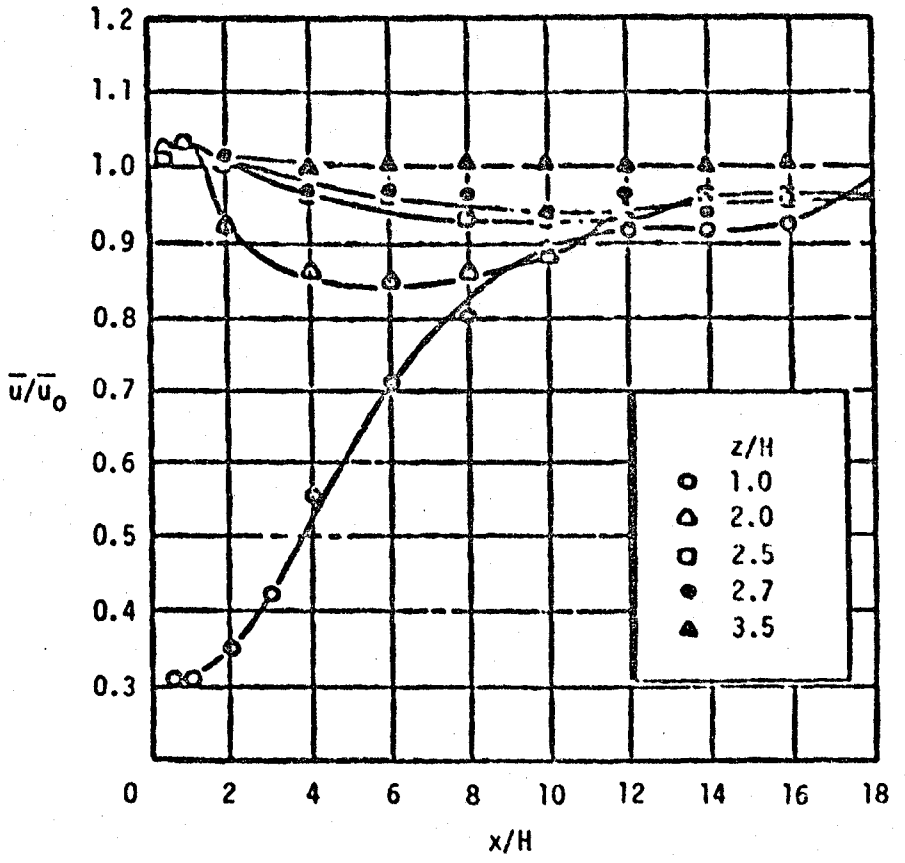

Figure 6.2. Velocity ratio at y/H = 0 for block aspect ratio = 2.44.

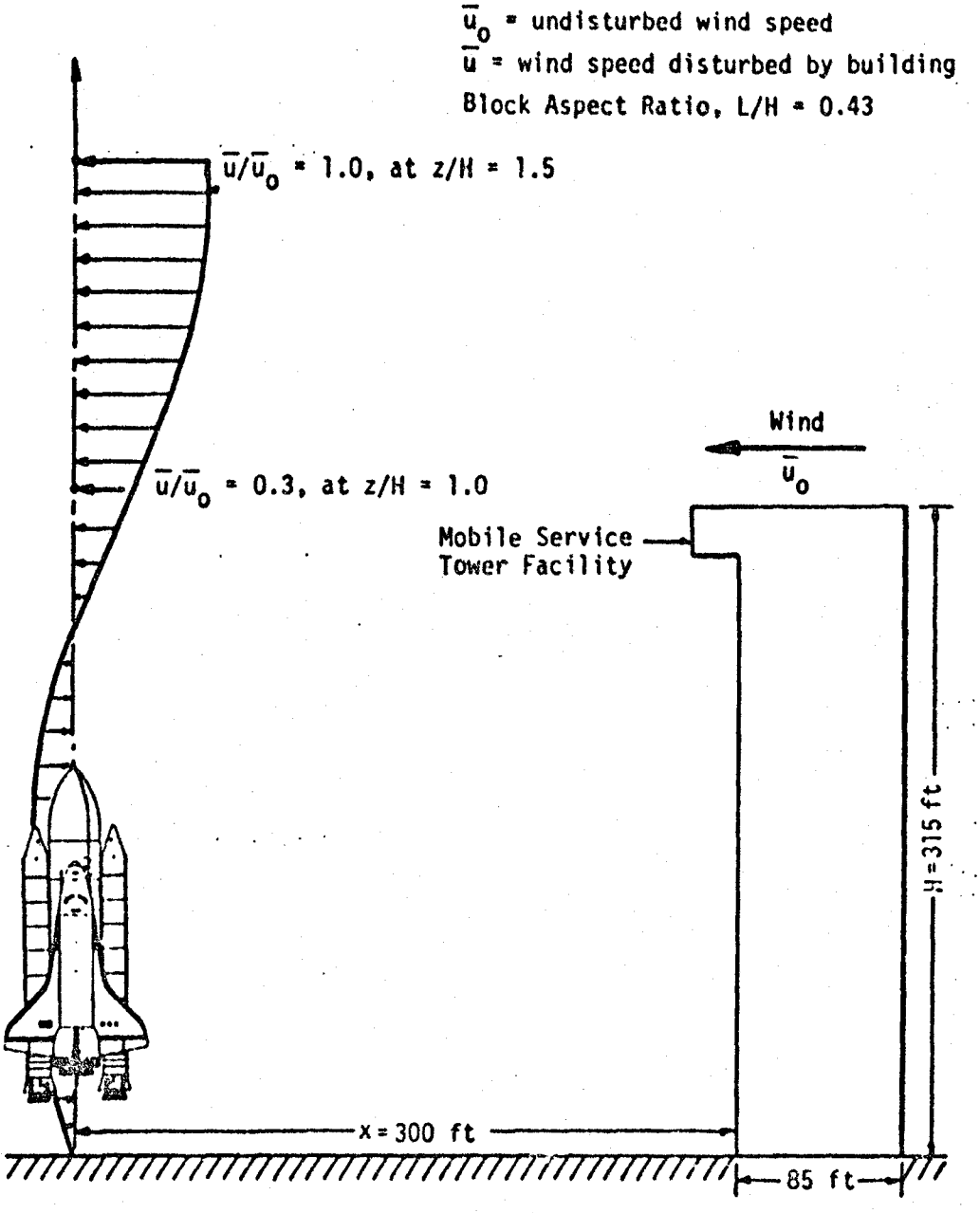

Figure 6.3. Wind bending load on space shuttle which is induced by mobile service tower.

7.0 TURBULENCE

In addition to the mean velocity pattern over the natural and man-made terrain features, the turbulence flow associated with high-frequency fluctuation is also an important factor to be considered in space shuttle launches. Neal et al. (1981) carried out a wind tunnel boundary layer simulation of wind flow over complex terrain. Figures 7.1 and 7.2 show the isotach and isoturb contour plots. The results show that velocities in excess of 0.9 of the gradient velocity occur in the bottom of the boundary layer on the top of the saddle. Also, significant turbulence intensity always occurs to the downstream flow (even upstream flow) of the model. Recalling the flow patterns around the launch pad (Section 5.0), the space shuttle is possibly shrouded in the wake region behind the block terrain. Thus, the significant shear layer in the wake will induce uneven stressing of the shuttle.

It is known that the prevailing wind direction at VAFB (SLC-6) is mainly from the northwest (i.e., onshore wind). When air moves from water to land, many surface properties change and an internal boundary layer develops. The air within this layer is modified by the new surface, whereas the air above it essentially retains its upstream properties. Elliott (1958) found that the height h of the interface between these two regions is given by

$$\frac{h}{z_0} = a\left(\frac{x}{z_0}\right)^{0.8}$$

where $a = 0.75 + 0.03\ \ln(z_0'/z_0)$ and z_0 and z_0' are upwind and downwind roughness lengths, respectively.

Panofsky et al. (1981) measured the spectrum over land downwind of water at Riso. Figure 7.3 shows u-velocity spectra at a height of 2 m for near-neutral conditions over water (Mast 0) and 70 m downwind of the shoreline (Mast 2A). The height of the interface at 70 m downwind of the shoreline is about 6 m > 2 m. The figure shows that there is no significant difference between the two spectra at low frequencies.

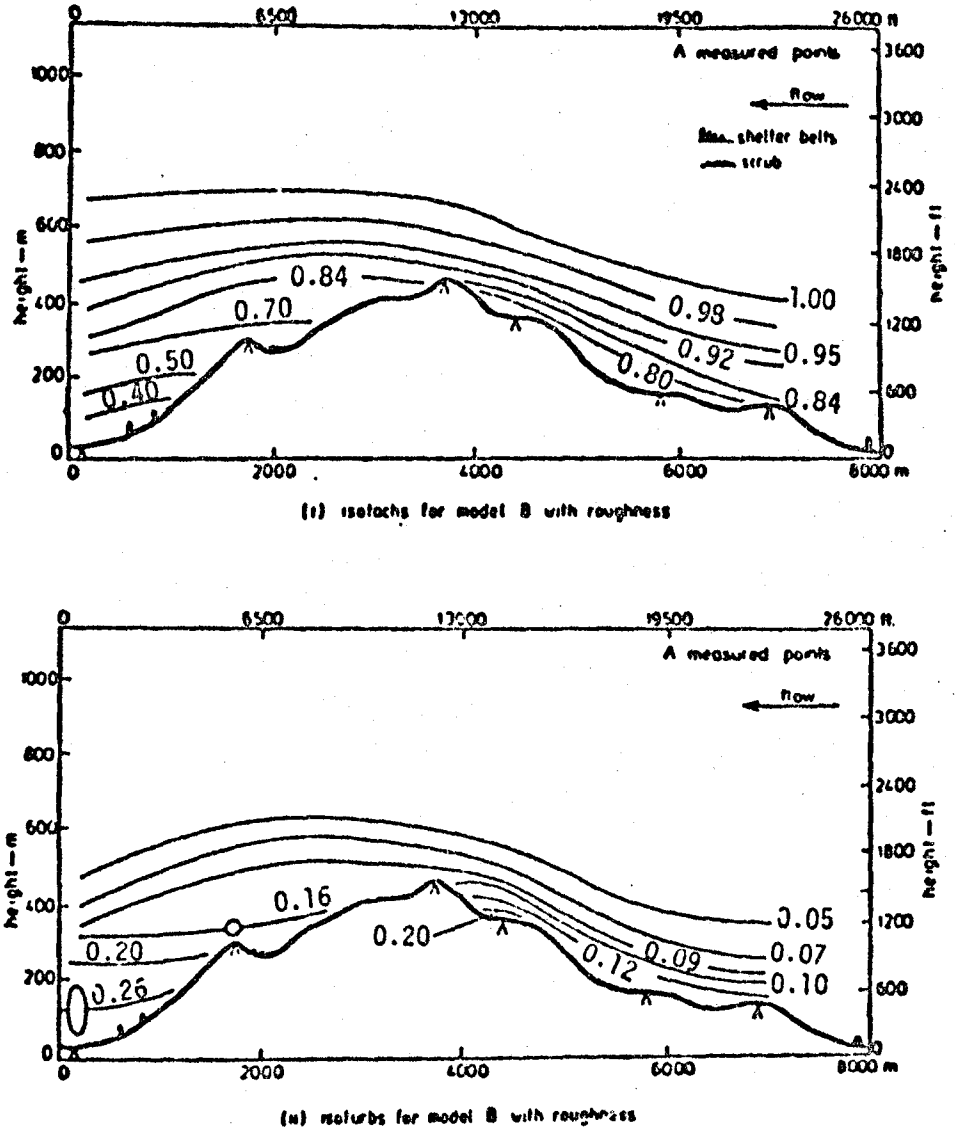

Figure 7.1. Isocontour graphs for longitudinal cross section YY.

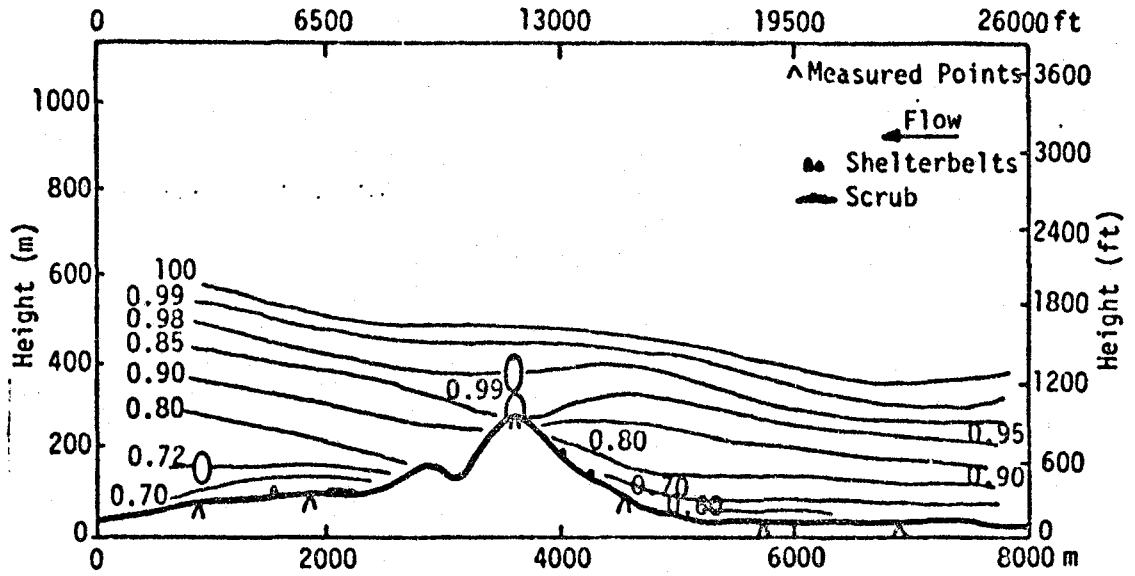

(a) Isotachs for Model B with roughness.

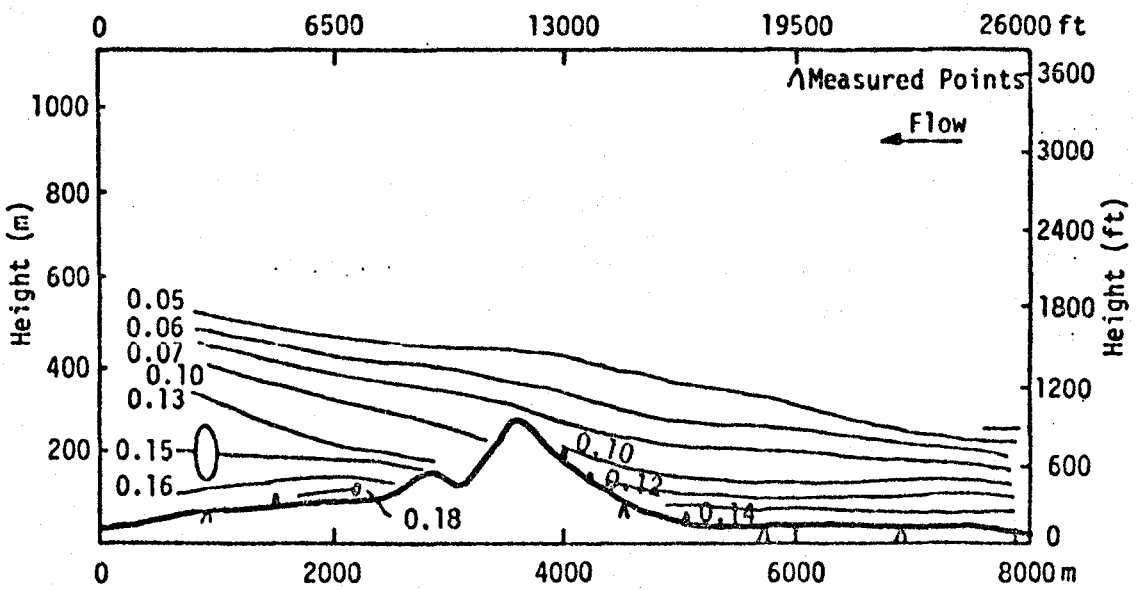

(b) Isoturbs for Model B with roughness.

Figure 7.2. Isocontour graphs for longitudinal cross section UU.

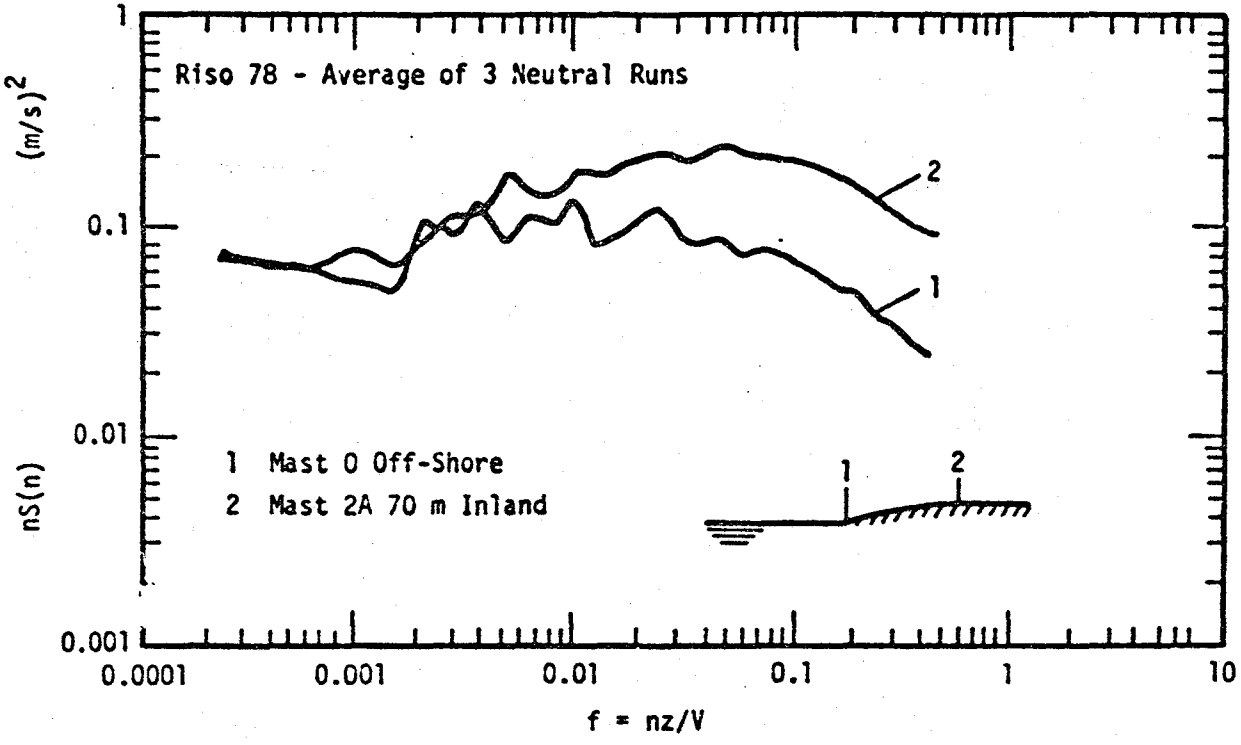

Figure 7.3. Average spectra for the u component in near-neutral conditions 2 m above water and land at Riso.

However, the increased roughness of the land has produced increased spectral densities at high frequencies. Figure 7.4 shows average spectra of the three velocity components in near-neutral conditions. In each case, the spectra on the inland mast (2A) at heights of 8 m and 12 m are not significantly different from upstream (Mast 0, see Figure 7.3) spectra at 2 m. This is consistent with the fact that these heights are above the interface. At a height of 4 m, just below the interface, a slight increase is apparent in the high-frequency portion of the longitudinal spectrum but this increase is not easily distinguished in the other two components. At the 2 m height, the high-frequency portion of all components has been strongly increased above their upstream levels. The low-frequency ends of the spectra are characteristically noisy but clearly are unaffected by the roughness change. The spectra of all three components are significantly higher than Kaimal's spectrum of turbulence over flat terrain for frequencies less than about 0.04.

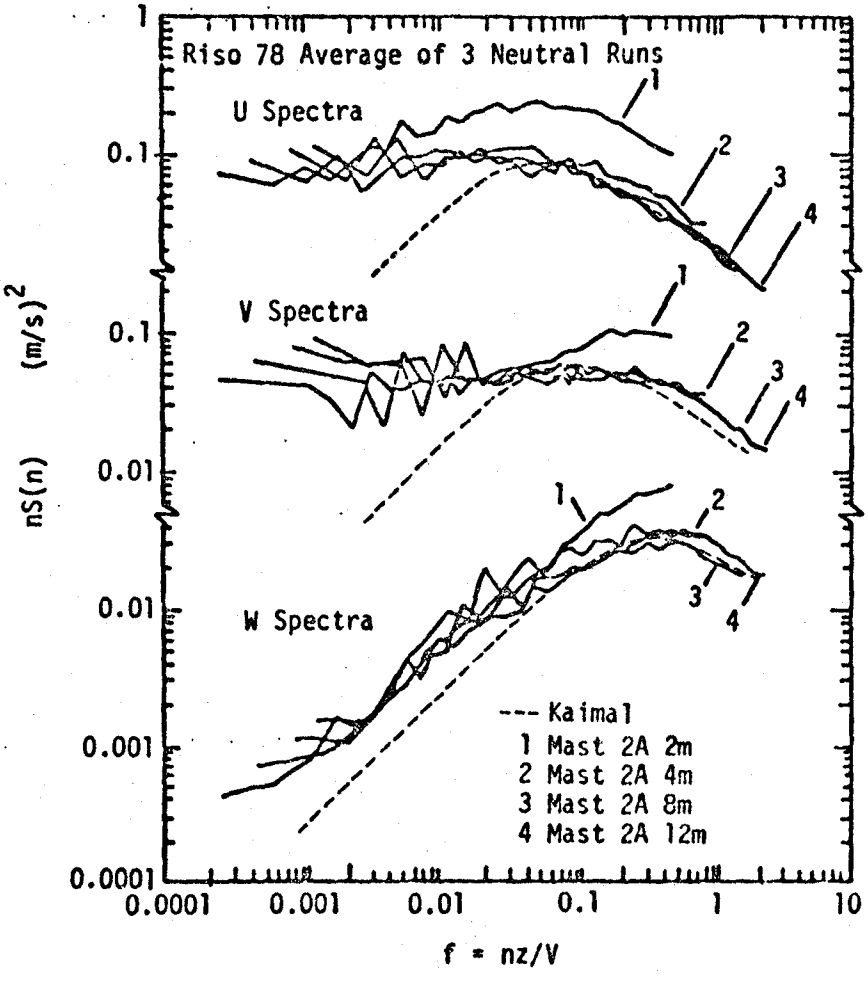

Figure 7.4. Average spectra for the three wind components in near-neutral conditions, at heights of 2, 4, 8, and 12 m, 70 m inland at Riso.

8.0 CONCLUSIONS AND RECOMMENDATIONS

Based on the review of the flow characteristics over natural and man-made complex terrain, the terrain features around VAFB (SLC-6) will have a significant effect on the wind pattern at the launch site. Moreover, the vortices shed by the high building (i.e., mobile service tower) and other structures can create unusual wind loads on the space shuttle dwelt on the launch pad and during initial liftoff. Also, the terrain surface roughness and complex land patterns at VAFB launch area will produce increased turbulence energy at high and intermediate frequencies. Finally, the limited tower data show that correlation between the towers around SLC-6 correlates well in velocity and direction.

To quantify the magnitude of the wind loads on the space shuttle, additional measurements and analyses are required. Two methods are recommended which will provide insight and/or measurements (data) which can be used to accomplish the required additional analysis.

Method 1: Water tunnels have been used for many years in a research mode, primarily for investigating fluid flow behavior. Such a facility for visual and computational techniques to simulate atmospheric dispersion is presently being developed by FWG Associates, Inc. of Tullahoma, Tennessee. This facility has potential applications for observation and for measuring the complex flow patterns due to different terrain features. Thus, the flow patterns for the VAFB (SLC-6) launch area could be simulated and even quantified by use of this water tunnel facility.

Method 2: NASA B-57B instrumented aircraft has been involved in several field test programs for many years. A flight pattern designed properly could be used to investigate the mountain effects on the flow nature at the VAFB (SLC-6) launch site. The flow structure around the early flight path is also achievable from the flight test. And then, the characteristics of the turbulent flow which is very important to space shuttle launches are to be possibly and correctly evaluated by the flight test data.

REFERENCES

Defant, F. (1951). "Local Winds," in Compendium of Meteorology. American Meteorological Society, Boston, Mass., pp. 655-672.

DeMarrais, G. A., G. D. Holzworth, and C. R. Hosler (1965). "Meteorological Summaries Pertinent to Atmospheric Transport and Dispersion Over Southern California," U.S. Dept. of Commerce Tech. Paper No. 54, Washington, D.C.

Elliott, W. O. (1958). "The Growth of the Atmospheric Internal Boundary Layer," Trans. Am. Geophys. Union, 39:1048-1054.

Frost, W. and G. W. Frost (1984). "Velocity Correlation Between Towers on Vandenberg Air Force Base, California," Presentation to the Space Division Headquarters, U.S. Air Force, Los Angeles, Calif., October.

Frost, W., and C. F. Shieh (1981). "Guidelines for Siting WECS Relative to Small-Scale Terrain Features," Final report for Dept. of Energy/Battelle, Richland, Washington, under Contract EY-76-C-06-2443 (December).

Hansen, C. A., and J. E. Cermak (1975). Vortex-Containing Wakes of Surface Obstacles, Report #29, Colorado State University, Ft. Collins, Colorado.

Lea, D. A. (1969). Some Climatological Aspects of Santa Anas at Point Mugu, Pacific Missile Range, Point Mugu, Calif., February.

Lemburg, R. (1973). On the Wakes Behind Bluff Bodies in a Turbulent Boundary Layer, Report BLWT-3-73, University of Western Ontario, London, Ontario.

Leutheusser, H. J., and W. D. Baines (1967). "Similitude Problems in Building Aerodynamics," in Proceedings. Journal of Hydraulic Division ASCE, pp. 35-49, American Society of Civil Engineers.

Meroney, R. N., et al. (1978). "Sites for Wind Power Installations: Physical Modeling of the Influence of Hills, Ridges, and Complex Terrain on Wind Speed and Turbulence," RLO/2438-77/3, available from NTIS, Springfield, Va.

Meteorology Research, Inc. (1975). Meteorological Data Requirements Study for System Space Transportation Operations at Vandenberg Air Force Base, California, May.

Neal, D., et al. (1981). "A Wind Tunnel Boundary Layer Simulation of Wind Flow Over Complex Terrain: Effect of Terrain and Model Construction," Boundary-Layer Meteorology, 21:271-293.

Ostrowski, J. S., R. D. Marshall, and J. E. Cermak (1967). "Vortex Formation and Pressure Fluctuations on Buildings," Paper presented at the International Research Seminar on Wind Effects on Buildings and Structures, Ottawa, Canada, September 11-15.

Panofsky, H. A. et al. (1981). "Spectra Over Complex Terrain," The Penn. State University, University Park, Pa. 16801.

Schocker, Gordon (1984). Personal communications.

Simiu, E., and R. H. Scanlan (1978). Wind Effects on Structures: An Introduction to Wind Engineering. New York: John Wiley & Sons, Inc.

U.S. Navy (1956). Marine Climate Atlas of the World, Volume II, North Pacific Ocean, published by direction of the Chief of Naval Operations, NAVAER 50-1c-529, July 1.

U.S. Weather Bureau and California State Dept. of Public Health (1962). "Inversion and Upper Wind Data Study," unpublished manuscript.

Woo, H. B., J. A. Peterka, and J. E. Cermak (1977). "Wind-Tunnel Measurements in the Wakes of Structures," NASA CR-2806.

Yoshino, M. M. (1975). Climate in a Small Area. Tokyo: University of Tokyo Press.

END

DATE

FILMED

MAR 28 1985